



HAL
open science

Quantitative proteomics reveals the Sox system's role in sulphur and arsenic metabolism of phototroph *Halorhodospira halophila*

Giulia d'Ermo, Stéphane Audebert, Luc Camoin, Britta Planer-Friedrich, Corinne Casiot, Sophie Delpoux, Régine Lebrun, Marianne Guiral, Barbara Schoepp-Cothenet

► To cite this version:

Giulia d'Ermo, Stéphane Audebert, Luc Camoin, Britta Planer-Friedrich, Corinne Casiot, et al.. Quantitative proteomics reveals the Sox system's role in sulphur and arsenic metabolism of phototroph *Halorhodospira halophila*. *Environmental Microbiology*, 2024, 26 (6), pp.e16655. 10.1111/1462-2920.16655 . hal-04620414

HAL Id: hal-04620414

<https://hal.science/hal-04620414v1>

Submitted on 11 Oct 2024

HAL is a multi-disciplinary open access archive for the deposit and dissemination of scientific research documents, whether they are published or not. The documents may come from teaching and research institutions in France or abroad, or from public or private research centers.

L'archive ouverte pluridisciplinaire **HAL**, est destinée au dépôt et à la diffusion de documents scientifiques de niveau recherche, publiés ou non, émanant des établissements d'enseignement et de recherche français ou étrangers, des laboratoires publics ou privés.




Distributed under a Creative Commons Attribution - NonCommercial - NoDerivatives 4.0 International License

RESEARCH ARTICLE

ENVIRONMENTAL MICROBIOLOGY



Quantitative proteomics reveals the Sox system's role in sulphur and arsenic metabolism of phototroph *Halorhodospira halophila*

Giulia D'Ermo¹ | Stéphane Audebert² | Luc Camoin² |
 Britta Planer-Friedrich³ | Corinne Casiot-Marouani⁴ | Sophie Delpoux⁴ |
 Régine Lebrun⁵ | Marianne Guiral¹ | Barbara Schoepp-Cothenet¹ 

¹Aix-Marseille Université, CNRS, BIP-UMR 7281, Marseille, France

²Aix-Marseille Université, Inserm, CNRS, Institut Paoli-Calmettes, CRCM, Marseille Protéomique, Marseille, France

³Environmental Geochemistry, Bayreuth Centre for Ecology and Environmental Research (BAYCEER), University of Bayreuth, Bayreuth, Germany

⁴Laboratoire HydroSciences Montpellier, Univ. Montpellier, CNRS, IRD, Montpellier, France

⁵Aix-Marseille Université, CNRS, IMM-FR3479, Marseille Protéomique, Marseille, France

Correspondence

Barbara Schoepp-Cothenet and Marianne Guiral, Aix-Marseille Université, CNRS, BIP-UMR 7281, Marseille, France.
 Email: schoepp@imm.cnrs.fr and guiral@imm.cnrs.fr

Funding information

Aix-Marseille University; Institut Paoli-Calmettes, Centre de Recherche en Cancérologie de Marseille, IBISA (Infrastructures Biologie Santé et Agronomie); Cancéropôle PACA, FEDER projet Fight Cancer, the Provence-Alpes-Côte d'Azur Région; Région Provence-Alpes-Côte d'Azur and the company GERME S.A. (Marseille)

Abstract

The metabolic process of purple sulphur bacteria's anoxygenic photosynthesis has been primarily studied in *Allochromatium vinosum*, a member of the *Chromatiaceae* family. However, the metabolic processes of purple sulphur bacteria from the *Ectothiorhodospiraceae* and *Halorhodospiraceae* families remain unexplored. We have analysed the proteome of *Halorhodospira halophila*, a member of the *Halorhodospiraceae* family, which was cultivated with various sulphur compounds. This analysis allowed us to reconstruct the first comprehensive sulphur-oxidative photosynthetic network for this family. Some members of the *Ectothiorhodospiraceae* family have been shown to use arsenite as a photosynthetic electron donor. Therefore, we analysed the proteome response of *Halorhodospira halophila* when grown under arsenite and sulphide conditions. Our analyses using ion chromatography-inductively coupled plasma mass spectrometry showed that thioarsenates are chemically formed under these conditions. However, they are more extensively generated and converted in the presence of bacteria, suggesting a biological process. Our quantitative proteomics revealed that the SoxXYZB system, typically dedicated to thiosulphate oxidation, is overproduced under these growth conditions. Additionally, two electron carriers, cytochrome *c*_{551/c}₅ and HiPIP III, are also overproduced. Electron paramagnetic resonance spectroscopy suggested that these transporters participate in the reduction of the photosynthetic Reaction Centre. These results support the idea of a chemically and biologically formed thioarsenate being oxidized by the Sox system, with cytochrome *c*_{551/c}₅ and HiPIP III directing electrons towards the Reaction Centre.

INTRODUCTION

The *Ectothiorhodospiraceae* and the *Halorhodospiraceae* thrive in saline waters throughout the world, with a preference for alkaline soda lakes (Imhoff et al., 2022). Together with the *Chromatiaceae*, they include Purple

Sulphur Bacteria (PSB), which share with the Green Sulphur Bacteria (GSB) the ability to feed their photosynthesis by oxidizing sulphur compounds. While the *Chromatiaceae* produce internal sulphur globules, which are a transient form of sulphur storage during growth, *Ectothiorhodospiraceae* and *Halorhodospiraceae*

This is an open access article under the terms of the [Creative Commons Attribution-NonCommercial-NoDerivs](https://creativecommons.org/licenses/by-nc-nd/4.0/) License, which permits use and distribution in any medium, provided the original work is properly cited, the use is non-commercial and no modifications or adaptations are made.

© 2024 The Author(s). *Environmental Microbiology* published by John Wiley & Sons Ltd.



deposit external sulphur globules as the GSB do (Frigaard & Dahl, 2009). The oxidation of sulphur compounds has been extensively studied in *Chromatiaceae* and GSB. Therefore, the sulphur substrates sustaining growth, the subsequently released products and the enzymes involved in this energy metabolism are well known in these two latter groups (see, for reviews, Frigaard & Dahl, 2009; Kushkevych et al., 2021). Comparatively, little information is currently available on *Ectothiorhodospiraceae* and *Halorhodospiraceae*, apart from being known as predominantly strict anaerobes and phototrophs using most commonly sulphide (HS^-), thio-sulphate ($\text{S}_2\text{O}_3^{2-}$) and elemental sulphur (S^0) as photosynthetic electron donors, in most cases oxidized up to sulphate (SO_4^{2-}) (Imhoff et al., 2022). Very few investigations have been carried out on deciphering the photo-oxidation pathway of reduced sulphur compounds and models are based on genomic analyses only (Frigaard & Dahl, 2009; Imhoff et al., 2022).

In addition to the use of reduced sulphur compounds in photosynthesis, some *Ectothiorhodospiraceae* and *Halorhodospiraceae* members have been shown capable of growing by anoxygenic photosynthesis in the presence of arsenite (Budinoﬀ & Hollibaugh, 2008; Hernandez-Maldonado et al., 2017; Hoeft McCann et al., 2016; Kulp et al., 2008; Szyttenholm et al., 2020). Arsenic (As) is a highly toxic and widely distributed compound in the environment due to both geological and anthropogenic activities. It is found in both organic and inorganic forms and diverse redox states resulting from both abiotic and biotic processes. Inorganic oxyanions arsenite (H_3AsO_3) and arsenate ($\text{HAsO}_4^{2-}/\text{H}_2\text{AsO}_4^-$) are considered to be of greatest concern due to their toxicities and mobilities. While many microorganisms are described for As-resistance processes such as methylation or oxidation-reduction (for reviews, see Ben Fekih et al., 2018; Raturi et al., 2023; Shi et al., 2020), some prokaryotes can thrive on arsenic, by oxidizing arsenite or respiring arsenate (for reviews, see Kumari & Jagadevan, 2016; Oremland et al., 2017; van Lis et al., 2013), using three different Molybdenum enzymes: the arsenite oxidases Aio and Arx and the arsenate reductase Arr. In the case of anaerobic photosynthesis in *Ectothiorhodospiraceae* and *Halorhodospiraceae*, the enzyme shown to be responsible for the arsenite oxidation is the Arx (Hernandez-Maldonado et al., 2017; Szyttenholm et al., 2020; Zargar et al., 2012) but here again, no details on the pathway are known.

The present study aimed to fill the gap of knowledge on the *Halorhodospiraceae* photosynthetic sulphur metabolism at the molecular level, and to make progress in the understanding of the use of arsenite in anaerobic photosynthesis. With this goal, we deciphered the photosynthetic metabolism of *Halorhodospira (H.) halophila* SL1, an extremophilic strict both anaerobic and phototrophic PSB growing optimally at

130 g.L^{-1} NaCl, pH 8.8 and 42°C . The genomic sequence of *H. halophila* SL1 was published in 2013 (Challacombe et al., 2013) and only partially analysed in 2022. Such analysis did not allow the identification of functional proteins under photosynthesis (Imhoff et al., 2022). Two studies identifying and characterizing specific proteins involved in photosynthesis of *H. halophila* SL1 (Lieutaud et al., 2005; Schoepp-Cothenet et al., 2009) sketched the current draft model presented in Figure 1: a cyclic electron transfer takes place between a cytochrome bc_1 complex and a photosynthetic Reaction Centre (RC of Type-II i.e., using quinones), with the intermediate electron transporters being both a soluble HiPIP II (for High Potential Iron-Sulphur Protein) and a membrane diffusible menaquinone (MK) pool. In the case of *H. halophila* (and other sulphur oxidizing bacteria), the HiPIP II does not directly reduce the bacteriochlorophyll special pair (P) of the RC but instead, a tetrahemic cytochrome subunit of the RC that in turn reduces P (Lieutaud et al., 2005). Since *H. halophila* is a sulphur oxidizing phototroph using an RC-II, electrons are presumably coming from both periplasmic systems, enabling a direct reduction of the RC, and from membranous systems reducing the MK pool (see for general principle [Frigaard & Dahl, 2009; Kushkevych et al., 2021]). The cyclic electron flow allows the generation of a proton motive force (PMF) thanks to the activity of the cytochrome bc_1 complex and the RC. This PMF is further used for ATP synthesis and, together with the oxidation of the MK pool, for the production of reducing power in the form of NADH by a linear reverse electron flow. To go further in the reconstruction of the energy metabolism of the bacterium, we opted for a proteomic approach to complete the little information currently available (Lieutaud et al., 2005; Schoepp-Cothenet et al., 2009). We performed a mass spectrometry-based whole proteome analysis with label-free quantification of *H. halophila* phototrophically grown in the presence of various inorganic reduced sulphur compounds in the concomitant presence of sulphide and arsenite, to identify proteins (enzymes and electron carriers) involved in its photosynthetic metabolism.

EXPERIMENTAL PROCEDURES

H. halophila growth conditions

H. halophila SL1 (DSM 244) has been grown anaerobically and phototrophically at 42°C (in a thermostatically controlled oven under illumination of a filament lamp) in 100 mL bottles in basic medium derived from ATCC 1448 medium in which Vitamin solution was omitted, pH adjusted at 8.8 and NaCl added at 2.22 M ($=130 \text{ g.L}^{-1}$). Either 6 mM HS^- , 6 mM $\text{S}_2\text{O}_3^{2-}$, 62.5 mM ($=2 \text{ g.L}^{-1}$) S^0 , 2 mM sulphite

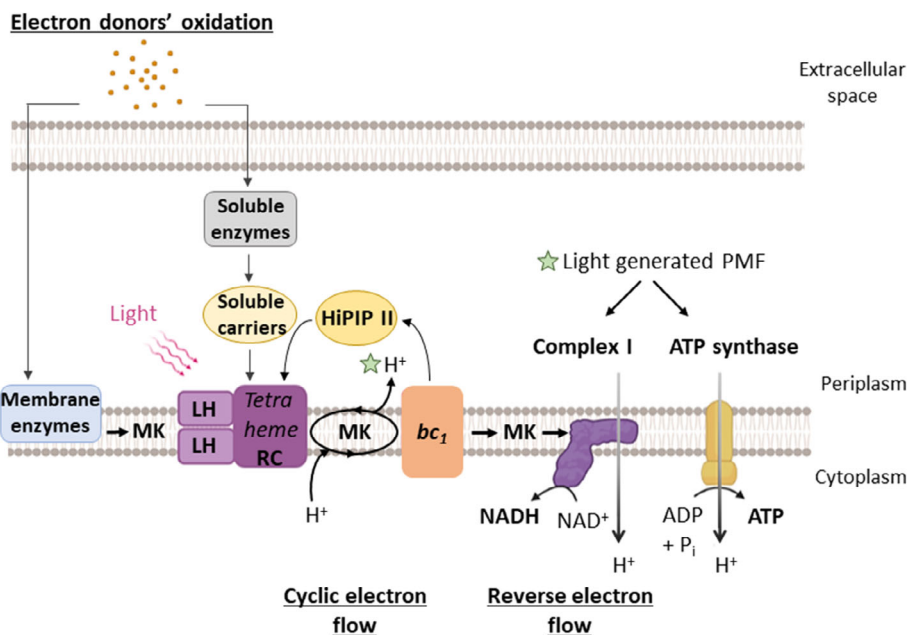


FIGURE 1 Scheme of the known and hypothesized electron donor's oxidation and photosynthetic pathway in *Halorhodospira halophila*. *bc₁*, cytochrome *bc₁* complex; *HiPIP II*, High Potential Iron Sulphur Protein II; *LH*, light harvesting complexes; *MK*, menaquinones; *PMF*, proton motive force; *RC*, reaction centre.

(hereafter SO_3^{2-}), 6 mM tetrathionate (hereafter $\text{S}_4\text{O}_6^{2-}$) or 6 mM HS^- /2 mM arsenite were added to the basic medium. Cultures were also performed on a basic growth medium with arsenite in place of the sulphur compound, with 1 mM added at the beginning of growth and then at 24, 55 and 95 h. Each growth was done in triplicate.

Membrane fragment preparation

For membrane fragments preparation, cells collected from cultures by 20 min centrifugation at 6000g and resuspended in 50 mM Tricine (pH 8) were broken by passing through a French press three times. Unbroken cells were eliminated by a 20-min centrifugation at 6000g, 4°C. Subsequent ultracentrifugation overnight at 180,000g, 4°C, separated the 'total soluble fraction' in the supernatant from the 'membrane fragments' in the pellet. The pellet was resuspended at 30 mg proteins.mL⁻¹ in 2.22 M NaCl/50 mM N-(2-Hydroxyethyl) piperazine-N'-(2-ethanesulfonic acid) (HEPES)/50 mM Tricine/50 mM N-(1,1-dimethyl-2-hydroxyethyl)-3-amino-2-hydroxypropanesulfonic acid (AMPSO) pH 8.8 (buffer A). This preparation constituted the crude membrane fraction containing significant amounts of HiPIP II (Lieutaud et al., 2005). Membranes depleted from HiPIP II were obtained by submitting the crude membrane fraction diluted 100 times in the same buffer to sonication and subsequent ultracentrifugation 2 h at 180,000g, 4°C.

Preparation of samples for proteomic analyses

Total protein extracts were prepared using 2×10^9 cells collected at the end of the exponential growth phase: 29 h under HS^- , 33 h under $\text{S}_2\text{O}_3^{2-}$, 56 h under S^0 , 55 h for arsenite alone and 71 h under HS^- + arsenite. Cell pellets were obtained by 20 min centrifugation at 12,000g at room temperature, washed in 50 mM Tricine pH 8 and stored at -20°C after a flash freeze in liquid nitrogen. Pellets have then been resuspended in 100 μL Lysis buffer (5% SDS, 50 mM Tricine pH 8) + DNase 5 μg.mL⁻¹ and 1 mM MgCl_2 and further probe sonicated to fully remove the DNA. Lysed cells were centrifuged for 8 min at 12,000g at 10°C to remove unbroken cells and recover the supernatants (total protein extracts). Protein extracts have been quantified using the BCA Protein Assay Kit (Sigma-Aldrich) and their quality was checked by migration on precast 4%–15% gradient SDS gel (Mini-PROTEAN TGX™ Protein Gels from Bio-Rad) and further visualization by silver staining (ProteoSilver™ Silver Stain Kit from Sigma-Aldrich). Each sample has been collected in biological triplicate.

Proteomic analysis

For relative proteomic analysis, proteins were solubilized in 15 μL of LDS sample buffer (2× concentrated), (Invitrogen, Life Technologies) before loading on



NuPAGE™ 4%–12% Bis–tris acrylamide gels according to the manufacturer's instructions (Invitrogen, Life Technologies). Running of samples was stopped as soon as proteins were stacked as a single band and following imperial blue staining (Life Technologies), the upper part of the gel containing the proteins was cut and processed for classical in-gel digestion (washes, thiols reduction with 10 mM DTT and cysteine alkylation with 55 mM iodoacetamide). Each band was further digested as previously described with trypsin and analysed by liquid chromatography (LC)-tandem MS (MS/MS) using a Q-Exactive plus Mass Spectrometer (Thermo Fisher Scientific, San Jose, CA) online with a nanoRSLC Ultimate 3000 chromatography system (Thermo Fisher Scientific, Sunnyvale, CA). First, peptides were concentrated and purified on a pre-column PepMap100 C18, 2 cm × 100 µm I.D., 100 Å pore size, 5 µm particle size in solvent A (0.1% formic acid in 2% acetonitrile). In the second step, peptides were separated on a reverse phase LC EASY-Spray C18 column PepMap RSLC C18, 50 cm × 75 µm I.D., 100 Å pore size, 2 µm particle size (Thermo Fisher) at 300 nL min⁻¹ flow rate and 40°C. After column equilibration peptides were eluted from the analytical column by a three-step linear gradient (2.5%–27.5% solvent B [80% acetonitrile 0.1% formic acid in water] for 100 min, 27.5%–40% for 20 min and a last elution 40%–90% for 2 min). For peptide ionization in the EASY-Spray nano-source in front of the mass spectrometer, the spray voltage was set at 2.2 kV and the capillary temperature at 275°C. The mass spectrometer was used in data-independent mode with the following parameters. First, MS spectra were acquired in the Orbitrap in the range of m/z 375–1500 at a FWHM resolution of 35,000 measured at 200 m/z. AGC target was set at 1 × 10⁶ with a Maximum Injection Time of 60 ms. MS2 spectra were acquired in the Orbitrap with a resolution of 17,500 after isolation of the parent ion in the quadrupole and fragmentation in the HCD cell under collision Energy of 27%. DIA parent ion range was from 400 to 1000 m.z.⁻¹ divided into 24 m.z.⁻¹ windows.

Proteomics data processing

Relative intensity-based label-free quantification (LFQ) was processed using the DIA-NN 1.8 algorithm. Raw files were searched against the *H. halophila* SL1 database extracted from UniProt on the 22nd of February 2022 and containing 2432 entries with the addition of a protein contaminant bank (Frankenfield et al., 2022). The following parameters were used for searches: (i) trypsin allowing cleavage before proline; (ii) one missed cleavage was allowed; (iii) cysteine carbamidomethylation (+57.02146) as a fixed modification and methionine oxidation (+15.99491) and N-terminal acetylation (+42.0106) as variable modifications; (iv) a

maximum of one variable modification per peptide allowed; and (v) minimum peptide length was 7 amino acids and a maximum of 30 amino acids. The match between runs option was enabled. The precursor false discovery was set to 1%. DIA-NN parameters were set on Single-pass mode for the Neural Network classifier, Robust LC High precision for quantification strategy and RT-dependent mode for Cross-run normalization. The library was generated using a Smart profiling setup. The main output file from DIA-NN was further filtered at 1% FDR and LFQ intensity was calculated using our DIAgui package at 1% *q*-value (<https://github.com/marseille-proteomique/DIAgui> [Gerault et al., 2024]). The statistical analysis was done with the Perseus program (version 1.6.15.0) (Tyanova & Cox, 2018). Quantifiable proteins were defined as those detected in above 70% of samples in at least one condition. Protein LFQ normalized intensities were base 2 logarithmized to obtain a normal distribution. Missing values were replaced using data imputation by randomly selecting from a normal distribution centred on the lower edge of the intensity values that simulate signals of low abundant proteins using default parameters (a downshift of 1.8 standard deviations and a width of 0.3 of the original distribution). To determine whether a given detected protein was specifically differential, a two-sample *t*-test was done using permutation-based FDR-controlled employing 250 permutations. DIAgui was also used to generate intensity-based absolute quantification (iBAQ) that roughly estimates the relative abundance of the proteins within each sample (Brønstrup, 2004; Schwanhauser et al., 2011). This intensity was used to calculate the proportion of some family proteins.

Enrichment analyses

A COG (Cluster of Orthologous Genes) functional annotation of *H. halophila* SL1 proteome deduced from genome analysis was performed through EggNOG Mapper v2.1.9. Functional enrichment analyses based on the COG classes were then performed on sets of differential proteins highlighted by the proteomic analysis, containing at least 100 proteins, compared to the total theoretical proteome.

Quantification of sulphur compounds

Sulphur compounds have been quantified in growth medium throughout cell growth by ion chromatography. Supernatants were collected by centrifugation at 12,000g for 20 min at room temperature, diluted 500× in 1% isopropanol, 0.22 µm filtered and injected at 1 mL.min⁻¹ on a Metrosep A Supp 4 column (250 × 4.0 mm) coupled to a precolumn cartridge



PRP-2 (Metrosep RP2 Guard/3.5) (Metrohm, Herisau Switzerland) at room temperature. The Metrohm 925 ECO ion chromatograph used is equipped with a conductivity detector and a Metrohm Suppressor Module (MSM) and allows the detection of SO_4^{2-} , SO_3^{2-} , $\text{S}_2\text{O}_3^{2-}$ and $\text{S}_4\text{O}_6^{2-}$ anions. The eluent (1.7 mM NaHCO_3 /1.8 mM Na_2CO_3 , 20% acetone) was filtered (0.22 μm) and degassed/sonicated before usage, whereas the suppressor regenerant solution (100 mM H_2SO_4) was only filtered. Quantifications were made by calibration using commercial compounds. Each quantification was done in triplicate. The instrument was controlled by the MagIC Net Basic software, which was used to evaluate the data.

For sulphide measurements, the growth supernatant was collected in a glove box, filtrated and immediately supplemented with 10 N NaOH (25 μL for 1 mL of the sample) before storage at -20°C . Sulphide was quantified by the methylene blue formation method, as follows (modified from Trueper & Schlegel, 1964). In a total volume of 1.2 mL, 200 μL 2% Zinc acetate was incubated with the sample (growth supernatant), 0.25 N NaOH, 100 μL 30 mM FeCl_3 prepared in 1.2 M HCl and 100 μL 20 mM *N,N*-Dimethyl-*p*-phenylenediamine dihydrochloride prepared in 7.2 M HCl, for 15 min in the dark at room temperature. The absorbance was measured at 670 nm against a blank. A standard curve, using a Na_2S solution deaerated with argon and prepared in 0.25 N NaOH, was performed for each assay.

Quantification of arsenic compounds

Determination of arsenite and arsenate concentrations was carried out by HPLC-ICP-MS (High-Performance Liquid Chromatography coupled to Inductively Coupled Plasma Mass Spectrometry). A 50 μL sample was injected into the HPLC system (ICS-5000 and autosampler AS-AP, Thermo Scientific). A strong anion-exchange Hamilton PRP-X100 column (250 \times 4.1 mm i.d. \times 10 μm , Interchim, Montluçon, France) and pre-column (Hamilton PRP-X100, 2 cm) were used and isocratic elution mode (30 mM $\text{NH}_4\text{H}_2\text{PO}_4$ /(NH_4) $_2\text{HPO}_4$ buffer, pH 8 + 2% Methanol HPLC grade, Carlo Erba). Detection of arsenite and arsenate was carried out using ICP-MS (iCAP-Qc, Thermo Fisher Scientific).

Quantification of arsenic species was made by external calibration using commercial solutions of arsenite (10 mg.L^{-1} arsenite in NaOH 0.5% and NaCl 0.1%, prepared with As_2O_3 99,99%) and arsenate (10 mg.L^{-1} arsenate in H_2O , prepared with As_2O_5 99,99%), both from CPACem (Trappes, France). These solutions were diluted daily with the mobile phase at concentrations of 5, 20 and 100 $\mu\text{g.L}^{-1}$. A commercial solution of germanium (50 $\mu\text{g.L}^{-1}$ Ge from SCP Sciences standard, in HNO_3 1%) was used as an internal standard by continuous addition through a

T-junction before introduction into ICP-MS, to correct for instrumental drift. The detection limits were determined daily and were generally lower than 0.1 $\mu\text{g.L}^{-1}$ for arsenite and 0.5 $\mu\text{g.L}^{-1}$ for arsenate.

The samples were kept frozen until analysis. Once thawed, samples were diluted twice in the mobile phase, to reach As species concentrations lower than 100 $\mu\text{g.L}^{-1}$. The quality of the analytical method was checked by analysing certified reference water (TM25.5, Environment Climate Change Canada LGC Standard); the sum of the concentration of arsenite and arsenate species in the certified reference water fell within the range of certified total As concentration value. Analytical error (relative standard deviation) was better than 5% for concentrations 10 times higher than the detection limits.

For thioarsenate species quantifications, samples (1 mL growth medium) were collected anaerobically in a glove box and immediately filtered through a 0.2 μm filter. HBED (10 mM stock solution in 10% ethanol adjusted at pH 8.8) was added up to 1 mM final concentration to complex Fe. The samples were then frozen in liquid nitrogen, shipped frozen, and stored at -20°C until analysis, basically as described in previous studies (Planer-Friedrich et al., 2007). After thawing the flash-frozen samples in a glovebox (95% N_2 /5% H_2), samples were diluted 500 times to have a maximum concentration for individual As species of 250 $\mu\text{g.L}^{-1}$. Arsenite, arsenate and the inorganic thioarsenates (Mono-, Di-, Tri- and Tetra-thioarsenates) were separated using an ion chromatography (940 Professional IC Vario Metrohm, Dionex AG/AS 16, 3–100 mM NaOH, flow rate = 1.2 mL.min^{-1}) coupled to an ICP-MS (Agilent 8900 ICP-QQQ). Dynamic reaction cell technology with oxygen as reaction gas was used to analyse As and S after mass-shift to $^{91}\text{AsO}^+$ and $^{48}\text{SO}^+$. Peak assignment was done based on previously reported retention times. Calibration was done using arsenite (NaAsO $_2$, Fluka) and arsenate ($\text{Na}_2\text{HAsO}_4 \times 7\text{H}_2\text{O}$, Fluka), and compound-independent calibrations were used to quantify inorganic thioarsenates via arsenate. Recovery of the reference material (TMDA 62.2, Environment Canada) in two separate runs was 110% and 112%. Signal drift was corrected by measuring a mid-range calibration standard every around 10 samples. Detection limits were $<0.1 \mu\text{g.L}^{-1}$.

Phase-contrast microscopy

H. halophila was cultivated as described above on HS^- , $\text{S}_2\text{O}_3^{2-}$, or S^0 . Samples were collected during and at the end of the exponential phase ($\text{OD}_{578} = 1.5$ –1.7 and $\text{OD}_{578} = 2$, respectively). Samples were put on a glass coverslip, gently squeezed under a 1 mm thick 1% agarose pad and directly imaged on an inverted



phase-contrast microscope (Nikon TiE) using an oil immersion 100 \times NA 1.45 objective, with 100–200 ms of exposure. Images were acquired using a cooled camera (Hamamatsu Orca Fusion). The acquisition was carried out using Nikon's NIS-Element software. Figures were finally processed through ImageJ.

In-gel arsenate reductase activity

Non-denaturing gels were inspired by Richey et al. (2009). SDS was replaced by Triton in a 5% acrylamide stacking and 10% acrylamide resolving gel. Membrane fractions (20 mg.mL⁻¹) were extracted for 30 min at 37°C with 1% (final concentration) Triton X-100. The supernatant obtained from a 10-min centrifugation at 12,000g was diluted in a loading buffer containing 0.1% Triton X-100. In gel arsenate reductase assays were performed under a nitrogen atmosphere in a Coy anaerobic dry box at pH 6 in 50 mM MES buffer, with 1 mM reduced (by Titanium citrate) methyl viologen as electron donor and 2 mM sodium arsenate as acceptor. The activity was observed on the gel by the destaining of reduced methyl viologen once oxidized in the band containing the enzyme.

Overproduction of soluble electron carriers

Genes for soluble carriers (cytochrome *c*₅₅₁/*c*₅ and HiPIP III) were cloned in *Escherichia* (*E.*) *coli* C600 using the pET-28a vector (Table S1). Genes were amplified by PCR using chromosomal DNA isolated (using the GenElute HP Plasmid MiniPrep Kit from Sigma-Aldrich) from *H. halophila* as a template, primers listed in Table S2 and Q5 DNA polymerase, following the NEB protocol including the High GC enhancer. The forward and reverse primers have been designed based on the publicly available chromosomal sequence of Hhal_0118 (for cytochrome *c*₅₅₁/*c*₅) and Hhal_2378 (for HiPIP III) genes and introducing NdeI and HindIII restriction sites at the 5' and 3' ends, respectively and deleting the Stop codons in both genes. pET-28a plasmid was used for the genes' expression with a 6-His tag sequence at the 3' end or without any tag (Table S1). Both the HiPIP III and the cytochrome *c*₅₅₁/*c*₅ are periplasmic proteins, the HiPIP III is predicted to use the Tat-dependent transport pathway while the cytochrome *c*₅₅₁/*c*₅ is predicted to use the Sec-dependent one. The translated proteins are therefore *in fine* matured with both the His-tag and the signal peptide at the N-terminal cleaved, leaving the His-tag at the C-terminal. The cloned nucleotide sequences were confirmed by sequencing by Genewiz.

Recombinant vectors were transferred in *E. coli* BL21(DE3) for protein production. For the cytochrome *c*₅₅₁/*c*₅ production, the pEC86 vector carrying *ccm*

genes for cytochrome maturation (Arslan et al., 1998) was co-transferred (Table S1). Transformants were grown in LB medium with 100 μ g.mL⁻¹ kanamycin and 80 μ M FeCl₃ (for production of HiPIP III) or with 50 μ g.mL⁻¹ kanamycin/35 μ g.mL⁻¹ chloramphenicol and 40 μ M FeCl₃ (for production of cytochrome *c*₅₅₁/*c*₅), during 24 h at 37°C. Cells were collected by centrifugation at 6000g, 10 min, at 4°C and resuspended in 10 mM Imidazole/500 mM NaCl/20 mM sodium phosphate pH 7.3 buffer. Cells were broken twice by passing through a French press. The crude extract was recovered as the supernatant of an ultracentrifugation at 180,000g, 1 h, at 4°C. It was subjected to an HIS-Select Nickel Affinity Gel (Sigma-Aldrich) column chromatography following the protocol from Sigma, with a protein elution in 100 mM Imidazole/500 mM NaCl/20 mM sodium phosphate pH 7.3 buffer. Fractions of eluted proteins were concentrated in ultrafiltration units (10 kDa cut off) and further purified onto a Sephadex G-100 size-exclusion column eluted with buffer A. Purity was checked by SDS electrophoresis.

Light-induced absorption spectroscopy

Light-induced absorption was measured with a double-beam JTS-10 (BioLogic) flash kinetics spectrophotometer as a difference between a reference and the photo-oxidized whole cells sample (Joliot et al., 1980). The whole cells were diluted in fresh growth medium devoid of any substrate and made anaerobic by waiting for oxygen consumption by the bacteria. The full oxidation of the photosynthetic system was obtained by an actinic light from a ring of diodes (800 nm). Changes in the absorbance at 420 nm, mainly originating from redox changes of cytochromes were followed. Changes in the absorbance in the alpha band, although more resolutive, were avoided because electrochromic absorption changes overlap the cytochrome absorption changes here (Lieutaud et al., 2005).

Optical redox titrations

Redox titrations were performed on purified proteins at room temperature as described by Dutton (Dutton, 1971) in buffer A, in the presence of the following redox mediators at 10 μ M: 2,5-dimethyl-*p*-benzoquinone; 2-hydroxy 1,2-naphthoquinone; 1,4-naphthoquinone; duroquinone and 2,5-dihydroxy-*p*-benzoquinone. Reductive titrations were carried out by using sodium dithionite, and oxidative titrations by using ferricyanide.

EPR spectroscopy

X-band cw EPR spectra were recorded on a Bruker Elexsys E500 spectrometer equipped with an

ER4012ST rectangular cavity fitted to an Oxford Instruments ESR900 liquid helium flow cryostat. Spectra were recorded at 15K, a microwave power of 6.3 mW, a microwave frequency of 9.44 GHz and a field modulation amplitude of 1 mT or 3.2 mT for HiPIP III or cytochrome c_{551}/c_5 , respectively. Illumination (5 min) was performed on reduced (with 5 mM ascorbate) membrane fragments diluted in buffer A and complemented or not with the purified electron carrier. During illumination, the EPR tube was kept in a water-ice bath to minimize the heating of the sample.

RESULTS

Growth conditions of *H. halophila* and observed metabolisms

H. halophila SL1 has been characterized as a strict sulphur oxidizing photosynthetic bacterium able to use HS^- , $\text{S}_2\text{O}_3^{2-}$ and S^0 as electron donors (Franz et al., 2009; Raymond & Sistrom, 1969). Some GSB or PSB were shown to use SO_3^{2-} or $\text{S}_4\text{O}_6^{2-}$ as well (Frigaard & Dahl, 2009), and we tried to grow *H. halophila* with these

compounds. This bacterium turned out not to grow on SO_3^{2-} , while it did on tetrathionate, which was however rapidly chemically transformed into $\text{S}_2\text{O}_3^{2-}$ (not shown) at the pH (8.8) and the temperature (42°C) used. These conditions, established as the optimum ones in our work, are slightly divergent from the ones established originally (pH 7.4–7.9 and temperature 47°C) (Raymond & Sistrom, 1969). The only three sulphur compounds that have been confirmed to be used and essential as electron donors to photosynthesis in *H. halophila* are therefore HS^- , $\text{S}_2\text{O}_3^{2-}$ and S^0 . While the most rapid growth has been observed on HS^- , almost identical maximum optical densities are reached under the three ‘sulphur conditions’ (Figure 2). With both HS^- and $\text{S}_2\text{O}_3^{2-}$, the most oxidized sulphur compound sulphate (SO_4^{2-}) was detected in the growth medium, as expected (Frigaard & Dahl, 2009). On $\text{S}_2\text{O}_3^{2-}$ we observed in addition the release of SO_3^{2-} traces (data not shown). In the case of S^0 , even though the same final OD was reached with slower growth, the generation of SO_4^{2-} was intriguingly low, even lower than that observed by Franz et al. (2009) (Figure 2). Deposition of extracellular sulphur globules as intermediates during growth on HS^- has been described for *Ectothiorhodospiraceae* and *Halorhodospiraceae*. These globules are

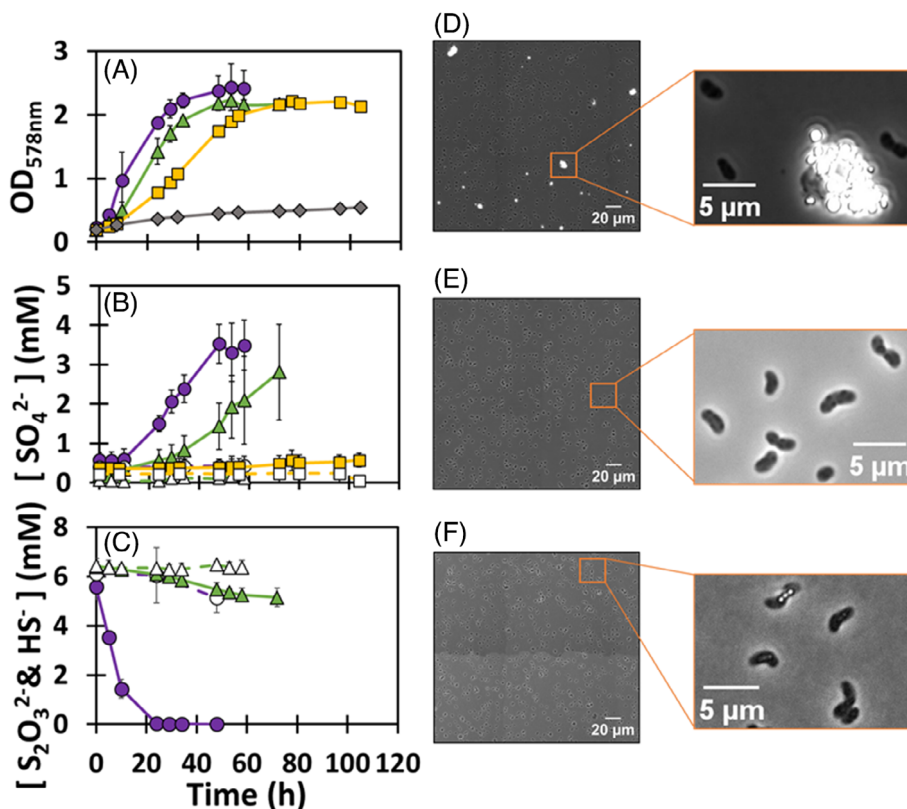


FIGURE 2 Photosynthetic growth of *Halorhodospira halophila* on sulphur compounds. Bacteria were grown either on HS^- (closed violet circles), $\text{S}_2\text{O}_3^{2-}$ (closed green triangles) or S^0 (closed yellow squares). (A) Growth curves. The grey curve corresponds to the growth without any substrate added. (B) SO_4^{2-} concentration in the growth medium for the three growth conditions. (C) $\text{S}_2\text{O}_3^{2-}$ and sulphide concentration in the growth medium for the growth on $\text{S}_2\text{O}_3^{2-}$ and the growth on HS^- , respectively. Abiotic controls are presented with corresponding open symbols and dashed lines. (D–F) Phase-contrast micrographs of the bacterium grown in the presence of HS^- (D), $\text{S}_2\text{O}_3^{2-}$ (E) or S^0 (F).

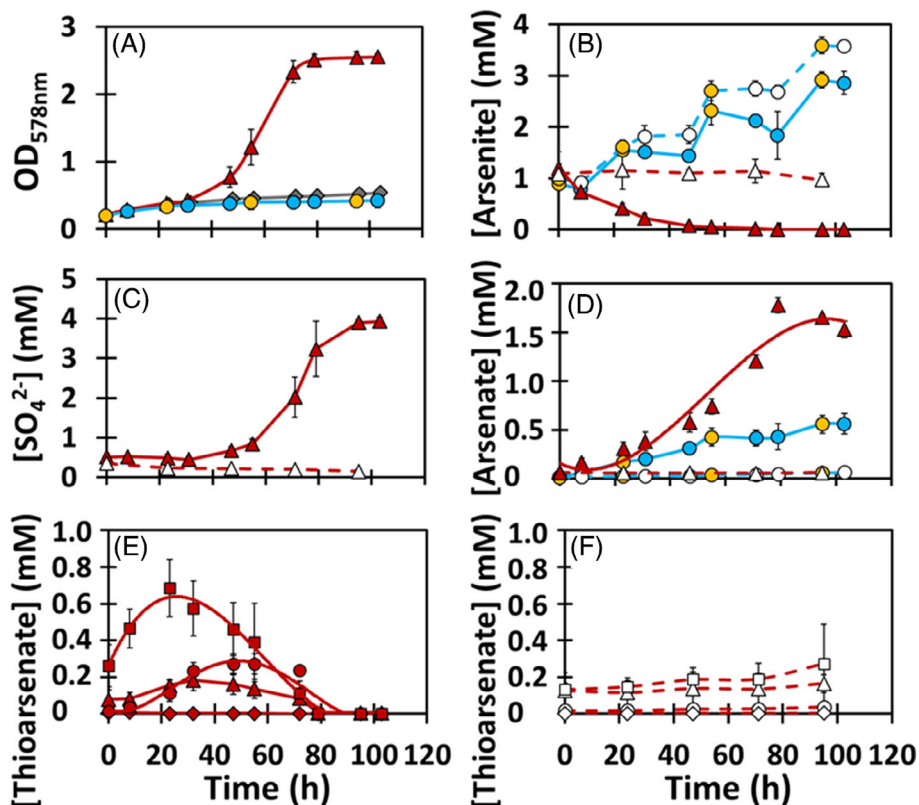


FIGURE 3 Photosynthetic metabolism of arsenite by *Halorhodospira halophila*. Bacteria were grown either on arsenite alone (closed blue circles) with 1 mM added at 0, 24, 55 and 95 h (addition time symbolized by closed orange circles), or on HS⁻ + arsenite (closed red triangles). (A) Growth curves. The grey curve corresponds to the growth without any substrate added. (B) Arsenite concentration in the growth medium. Open symbols represent abiotic controls corresponding to biotic conditions. (C and D) SO₄²⁻ and arsenate concentration in the growth medium, respectively. (E and F) Thioarsenates species concentrations in HS⁻ + arsenite condition, with panel (F) corresponding to the abiotic control and panel (E) to the biotic condition. Squares represent trithioarsenate, triangles represent dithioarsenate, circles represent the monothioarsenate while lozenges represent tetrathioarsenate.

further consumed and more or less totally (depending on the study) oxidized up to SO₄²⁻ (Frigaard & Dahl, 2009; Raymond & Sistrom, 1969). On the other hand, the storage of sulphur in globules is not always detectable or identified from S₂O₃²⁻ or S⁰ supplied for the growth of these bacteria. In the present work, phase-contrast microscopy, performed during *H. halophila* growth, confirmed that this strain does accumulate external sulphur globules from HS⁻ but not from S₂O₃²⁻ (Figure 2D,E). The globules appeared as agglomerates accumulated far from the cells and were consumed (no longer observable) at the end of growth (not shown). The release of SO₄²⁻ by *H. halophila* as an end-product in medium with HS⁻ was delayed and only started after 10 h of growth, reinforcing the hypothesis that the sulphur globules are a metabolic intermediate in this condition. Finally, cells grown on S⁰ showed astonishing images suggesting sulphur globules attached to the cells (or even internal) (Figure 2F). These globules, still observed in a late growth phase, would explain the virtual absence of SO₄²⁻ produced under this condition. Further experiments to confirm these observations are underway.

Two *Ectothiorhodospira* species, BSL-9 and PHS-1, have been published as able to grow on arsenite as the sole electron donor. *H. halophila*, however, seems unable to grow on arsenite alone, either provided at 2 mM at inoculation (Hoeft McCann et al., 2016; Szyttenholm et al., 2020) or provided at 1 mM along growth (this work, Figure 3A) even if a fraction of arsenite is oxidized into arsenate (Figure 3B). When 2 mM arsenite was supplemented with 6 mM HS⁻ (HS⁻ + arsenite condition), the growth was restored and SO₄²⁻ and arsenate (Figure 3C,D) are the final products, meaning that the two substrates have both been oxidized. A close examination of the kinetics of arsenite consumption and arsenate production revealed that from the initial 2 mM provided, As-species were transiently ‘missing’ during the growth. We therefore searched for transient formation of thiolated arsenic species, especially thioarsenates as set up by Planer-Friedrich et al. (2007). Monothioarsenate, dithioarsenate and trithioarsenate (Figure 3E,F) were indeed detected in the growth medium by anion exchange chromatography coupled to inductively coupled plasma mass spectrometry (IC-ICP-MS). Chemical formation of

thioarsenates from HS^- and/or $\text{S}(0)$ and arsenite is well documented (see Qing et al., 2023 and references herein) and several works reported the ability of bacteria to grow on monothioarsenate, among them *H. halophila* (Edwardson et al., 2014; Hartig et al., 2014; Planer-Friedrich et al., 2015). While some thioarsenate species are chemically formed (Figure 3F), a significantly larger amount is produced in the biotic experiment (Figure 3E) and is then converted to arsenate and SO_4^{2-} (see Figure 3C,D). The involved biological pathways are still unknown and abiotic decomposition of thioarsenates to arsenate and HS^- with subsequent bacterial oxidation of free HS^- to SO_4^{2-} , driving the chemical decomposition further, could be an alternative hypothesis. The absence of such a conversion of thioarsenates by the HS^- oxidizer *Allochromatium vinosum* shows, however, that the biological oxidation of HS^- is not sufficient to explain the decomposition of thioarsenates in biological samples (Edwardson et al., 2014).

The proteome of *H. halophila* SL1 in growing conditions

Global analysis of the proteome

To examine changes, with a special focus on bioenergetics, in response to different electron sources, we performed a whole-proteome profiling of *H. halophila* and compared the four phototrophic conditions enabling growth: HS^- , $\text{S}_2\text{O}_3^{2-}$, S^0 and HS^- + arsenite. In this study, we used a label-free proteomics approach using data-independent acquisition (DIA) mass spectrometry. DIA involves fragmenting all ions within a specific mass-to-charge ratio range (Gillet et al., 2012; Ludwig et al., 2018). DIA-MS offers high reproducibility, high proteomic depth and data completeness (Messner et al., 2023). We obtained indeed comprehensive proteomic data since, from a total of 2412 protein-coding sequences identified in the genome of *H. halophila*, with 1905 assigned to a putative function (Challacombe et al., 2013), a total of 2113 proteins (i.e., 88%) have been identified in our proteomic analysis. Up to 2031 common proteins (i.e., 96.2%, referred to as the core proteome), although varying in production level, were found in all four analysed conditions (Figure S1). The Principal Component Analysis (PCA) (Figure 4) showed very good reproducibility between the biological replicates and showed arsenic to have a specific effect on the proteome.

Phototrophic sulphur metabolism and other electron pathways

A global metabolic scheme can be predicted from the genomic sequence of *H. halophila* (Figure 5) and represents the first one for a *Halorhodospiraceae* member.

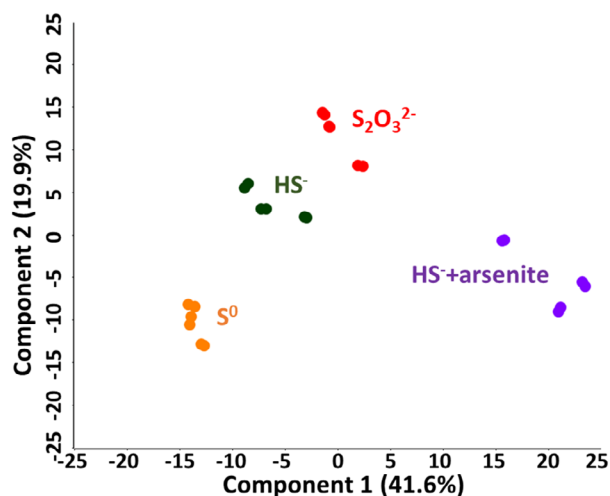


FIGURE 4 PCA Plot derived from the mass spectrometry analysis of the *Halorhodospira halophila* cells grown in the four culture conditions.

All the putative sulphur enzymes proposed to be involved in the sulphur substrates oxidation pathway were identified in the four conditions analysed: the sulphide: quinone oxidoreductase (Sqr, Hhal_1665), the dissimilatory sulphite reductase system (DsrABEFHCMKLJOPN, Hhal_1951-1963), the thiosulphate oxidizing Sox system (SoxXYZB, Hhal_1939-1942, Hhal_1948), the sulphite dehydrogenase (SoeABC, Hhal_1934-1936), the thiosulphate reductase (PhsABC, Hhal_1164-1166, in agreement with preceding annotation [Wells et al., 2019]) and three copies of flavocytochrome *c* sulphite dehydrogenase (FccAB, Hhal_1163, Hhal_1331 and Hhal_1945-1946). These enzymatic systems were produced together with the cytochrome *bc*₁ complex (Hhal_0182, Hhal_2107-2108) and the RC (Hhal_1603). The Sqr, Soe and possibly Dsr funnel the electrons from sulphur compounds to the quinone pool, thus likely feeding the cytochrome *bc*₁ complex for cyclic electron transfer with the RC, while Sox and Fcc would transfer the electrons directly to the RC through periplasmic soluble carriers. The role of Phs in this network is less straightforward (see below). It is to be noted that although *H. halophila* is not able to grow on SO_3^{2-} as mentioned above, this does not rule out the function of Soe as a true sulphite dehydrogenase as reported for *Aquifex aeolicus* (Boughanemi et al., 2020). SO_3^{2-} is the intracellular product of the Dsr system (Figure 5).

Surprisingly, the production of structural ArxB', ArxA, ArxB and ArxC proteins (Hhal_0352-0355) of the alternative arsenite oxidase Arx system (Table S3), together with the chaperone ArxD (Hhal_0356) was not regulated. Arx enzyme activity, detected in gel, on membrane fragments obtained from *H. halophila* grown under the various conditions tested confirmed the proteomic data, as the corresponding activity band is observable whatever the nature of the growth substrate (Figure S2A).

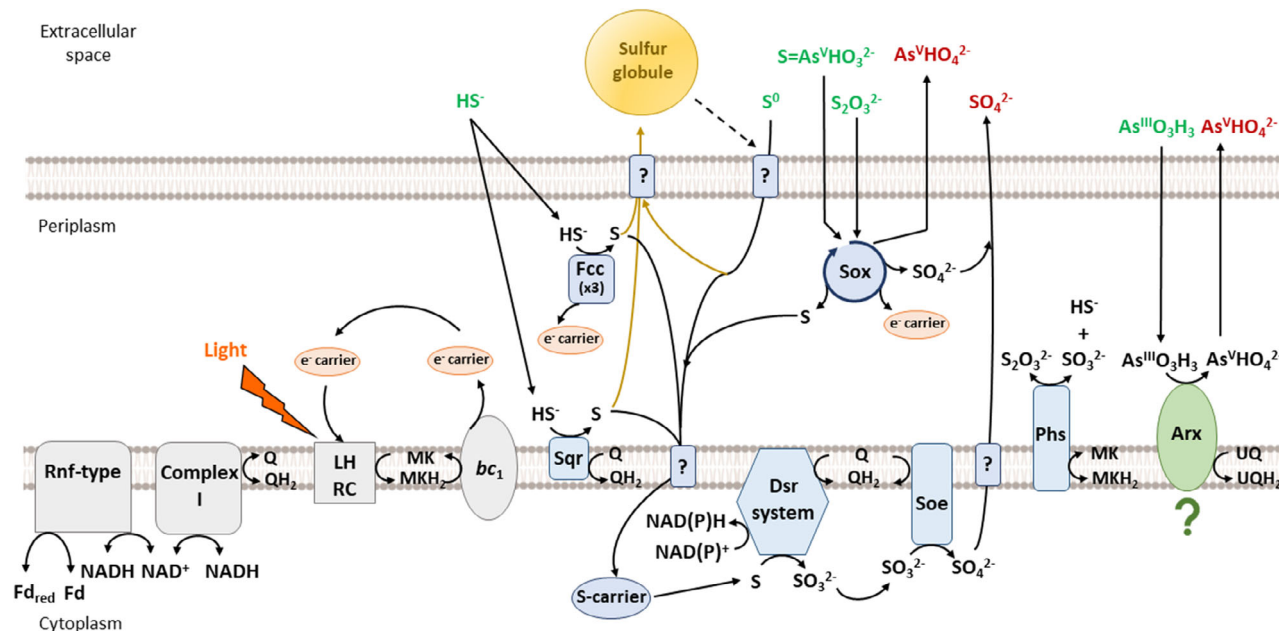


FIGURE 5 Photosynthetic metabolism of *Halorhodospira halophila* reconstructed from genomic and proteomic data. The PMF generated is used by the ATP synthase, not represented in this scheme, to produce ATP. $\text{As}^{\text{III}}\text{O}_3\text{H}_3$, $\text{S}=\text{As}^{\text{V}}\text{HO}_3^{2-}$, $\text{As}^{\text{V}}\text{HO}_4^{2-}$ and S correspond to arsenite, monothioarsenate, arsenate and S(0) respectively. bc_1 , cytochrome bc_1 complex; Fd and Fd_{red} , ferredoxin and reduced ferredoxin; LH , light harvesting complexes; MK , menaquinones; Q , quinones; RC , reaction centre; UQ , ubiquinones.

Consistent with the detection of both ubiquinone (UQ) and MK in *H. halophila* membranes (Szyttenholm et al., 2020), the core proteome contained both the Ubi and Men enzymes (Figure S3), with UbiU, UbiV and UbiT proteins (Hhal_1032-1034), dedicated to O_2 -independent UQ biosynthesis, in addition to the Ubil, UbiH and UbiF (Hhal_2225, Hhal_1186-1187), dedicated to O_2 -dependent UQ biosynthesis (Pelosi et al., 2019). It is noteworthy to mention in this context that under all growth conditions, a *bd*-type quinol oxidase (Hhal_2419-2420) was produced. Constitutive expression of genes coding for UbilHF and the *bd* oxidase, an enzyme with high affinity to O_2 proposed as a detoxification system rather than an energetic one for anaerobic bacteria (Murali et al., 2021), could confer an adaptative advantage to *H. halophila* to cope with trace amounts of O_2 .

The fact that Complex I (Hhal_1752-1765) was present in *H. halophila* whatever the conditions tested for growth, is in line with the scheme of a reverse electron transfer from the MK pool to the NAD^+ for the synthesis of reducing power (NADH) (Figure S3; Figure 5). In addition to Complex I, two other putative NAD^+ /NADH oxidoreductases (Hhal_0061-0067 and Hhal_0719-0723) with homologies to membrane-bound complexes of the Rnf-Nqr-Rsx type (reversible ferredoxin: NAD^+ oxidoreductase), were produced in all four growth conditions (Figure S3), raising the question of their function: complementing or competing with the Complex I for NADH synthesis.

In all four growth conditions, a plethora of electron carriers were produced (Figure S3). Two [2Fe-2S] ferredoxins (Hhal_0269 and Hhal_0545), and two [4Fe-4S] ferredoxins (Hhal_0271 and Hhal_1658), homologous to ferredoxins used by Rnf-type complexes, were identified. In addition, three HiPIPs (Hhal_1363, Hhal_2378 and Hhal_1624, denoted HiPIP II, III and IV hereafter) and four cytochromes *c* (Hhal_0118, Hhal_1169, Hhal_2381 and Hhal_2392) were found in this analysis. It is to be noted that both HiPIP III and HiPIP IV had escaped the eyes of researchers until now, HiPIP IV being the only one detected in the four growth conditions tested (Figure S3). For its part, the well-known HiPIP I (Hhal_1488) (Tedro et al., 1985) has never been retrieved in this whole-cell proteomic analysis.

The four cytochromes retrieved in the core proteome are not characterized in *H. halophila* SL1. The monohemic Hhal_1169 (hereafter called cytochrome chp) is predicted to bear a lipid anchor enabling it to cling to the membrane and Hhal_2392 is a putative soluble dihemic c_4 -like cytochrome. Chp and the monohemic Hhal_0118 (hereafter called c_{551}/c_5) are homologous to the soluble c_{551} characterized from *H. halophila* BN9626 and the c_5 from *Azotobacter vinelandii* (Bersch et al., 1996; Meyer, 1985) (Figure S4) and Hhal_2392 is homologous to the c_4 -type cytochrome from *Rubrivivax gelatinosus* (Ohmine et al., 2009). The putative multiheme cytochrome (Hhal_2381) is homologous to the decaheme MtrA/PioA involved in the metal


TABLE 1 Proteins with an increased abundance in HS⁻ condition (compared to S⁰ and S₂O₃²⁻).

Protein	Locus tag	S ⁰		S ₂ O ₃ ²⁻	
		Log ₂ (FC)	Log (p-value)	Log ₂ (FC)	Log (p-value)
DUF2345 domain-containing protein (VgrG2-like)	Hhal_0154	5.41*	9.09	>5.88*	10.47
Rhs element Vgr protein	Hhal_0155	5.28*	10.71	>4.77*	3.12
Hcp1-like protein	Hhal_0159	4.37*	9.95	5.41*	11.12
VipB/TssC-like protein	Hhal_0160	5.60*	10.20	>8.27*	10.39
VipA/TssB-like protein	Hhal_0161	5.79*	10.15	>6.66*	9.79
ImpA domain-containing protein (VasJ/TssA-like)	Hhal_0162	>4.93*	9.40	>4.84*	10.90
IcmF domain-containing protein (VasK/TssM-like)	Hhal_0163	5.92*	9.53	>5.31*	10.41
VasE/TssK-like protein	Hhal_0165	4.99*	8.24	>5.71*	10.37
Acr3 family transporter	Hhal_0197	2.53*	7.94	>4.77*	7.81
TonB-dependent receptor	Hhal_0387	2.96*	3.02	2.86**	2.87
Phage integrase family protein	Hhal_0746	>2.78*	6.62	>2.29**	7.73
Uncharacterized protein	Hhal_0927	3.10*	11.02	3.42*	7.16
Uncharacterized protein	Hhal_0929	>5.35*	8.59	>4.56*	7.60
DUF2169 domain-containing protein	Hhal_0930	>2.95*	4.94	>2.37**	5.67
Thiosulphate reductase PhsC-like subunit	Hhal_1164	2.10**	6.86	3.37*	7.14
Thiosulphate reductase PhsB-like subunit	Hhal_1165	1.84**	7.11	3.06*	6.74
Thiosulphate reductase PhsA-like subunit	Hhal_1166	2.06**	7.79	3.11*	10.02
Type II secretion system protein E/T4pilus PilB-like	Hhal_2020	4.79*	11.08	>4.37*	9.63
Single-stranded DNA-binding protein	Hhal_2184	2.20**	8.37	2.46**	9.25
Fimbrial protein pilin (ComP-like)	Hhal_2242	>3.85*	7.74	>3.71*	8.13
UPF0758 protein Hhal_2301	Hhal_2301	4.94*	6.75	>5.43*	6.70
DNA-protecting protein DprA	Hhal_2324	>4.14*	8.85	>4.13*	10.69
Mg-chelatase, subunit ChII	Hhal_2404	3.47*	10.49	4.67*	12.61

Note: > indicates that FC is virtual because it is derived by imputation of quantitative data.

Abbreviation: FC, fold change.

*q-Values (FDR) < 0.0001; S₀ = 2.

**q-Values (FDR) between 0.001 and 0.0001; S₀ = 2.

reduction/oxidation system Mtr/Pio/Omc, a porin-cytochrome complex facilitating electron transfer from/to extracellular substrates in various bacteria (Ross et al., 2007; White et al., 2016). The clustering of the gene coding for this multiheme cytochrome with homologues of *mtrB/pioB* (*hhal_2380* encoding a probable porin) and *mtrC/omcA* (*hhal_2379*) reinforces the identification here of a Mtr/Pio/Omc system. The presence, in this gene cluster, of HiPIP III (*hhal_2378*), a homologue of *pioC* from *Rhodospseudomonas palustris*, where PioC has been demonstrated to work in iron oxidation (Bird et al., 2014), is noteworthy.

Comparison of the proteome after growth with the three sulphur sources

From proteomic pairwise comparisons between the three sulphur compounds, no protein was found in significant (i.e., above the threshold) higher abundance in the proteome from bacteria grown with S₂O₃²⁻ compared to HS⁻ or S⁰ (Figures S5–S8), thus suggesting

either no protein to be specific for the S₂O₃²⁻ metabolism in *H. halophila* or these proteins to be constitutive. Twenty-three and seven proteins were however specifically and significantly (i.e., above the threshold) more abundant in the HS⁻ and in the S⁰ condition, respectively, in relation to the two other sulphur conditions (exhaustive lists of proteins in Tables 1 and 2; Figures S5–S8). All in all, this is indicative that there is likely no major change in the sulphur metabolism when *H. halophila* uses one of these inorganic compounds to thrive.

These quantitative proteomic data revealed a drastic increase in the abundance of a putative type VI secretion system (T6SS) (Hhal_0154–0155, Hhal_0159–0163, Hhal_0165) and some proteins of the Pili system under HS⁻ (Hhal_2020 and Hhal_2242) (Table 1). As shown above (Figure 2), the formation of external sulphur globules was at least higher, if not exclusively observed, in HS⁻ medium. The process of formation and mobilization of globules has not been studied in *Halorhodospiraceae*, but the need for enzymes/molecules secretion for the formation and degradation of these globules, as established


TABLE 2 Proteins with an increased abundance in S^0 condition (compared to HS^- and $S_2O_3^{2-}$).

Protein	Locus tag	HS^-		$S_2O_3^{2-}$	
		Log2 (FC)	Log (p -value)	Log2 (FC)	Log (p -value)
ABC-type glycine betaine transport system	Hhal_0235	2.00***	4.50	2.36*	6.57
Transcriptional regulator LysR family	Hhal_0341	2.66*	7.22	2.47*	8.34
Sulf_transp domain-containing protein	Hhal_0342	>4.48*	4.81	2.31***	4.78
Adenosine 5-phosphosulphate reductase	Hhal_1777	4.27*	3.69	>5.06*	8.07
Periplasmic binding protein	Hhal_1923	2.67*	9.02	2.08***	5.32
DrsE domain-containing protein	Hhal_1943	3.36*	8.62	3.55*	7.06
O-acetylhomoserine sulfhydrylase	Hhal_2153	2.57*	7.77	2.27*	9.13

Note: > indicates that FC is virtual because it is derived by imputation of quantitative data.

Abbreviation: FC, fold change.

* q -Values (FDR) < 0.0001; $S0 = 2$.

*** q -Value between 0.0011 and 0.0017; $S0 = 2$.

for *Acidithiobacillus ferrooxidans* (Beard et al., 2011), could rationalize the increase of the T6SS level under HS^- in *H. halophila*. To confirm this scheme, further investigations are required but it is to note that the absence of such external and distant sulphur globules under $S_2O_3^{2-}$ and S^0 (Figure 2) correlated with the lower production of T6SS and Pili in these conditions.

Comparison of the proteome under S^0 with the ones obtained under HS^- and $S_2O_3^{2-}$ (Table 2; Figures S5, S7 and S8) identified only seven proteins that are specifically more produced on S^0 in a statistically significant level. Among them are found a DsrE-like protein (Hhal_1943), CysH and CysB (Hhal_1777 and Hhal_0341), a putative membrane-bound sulphur transport protein (Hhal_0342) and an O-acetylhomoserine sulfhydrylase (Hhal_2153). Although the DsrE-like protein is conserved in the *Ectothiorhodospiraceae*, it has no equivalent in the model organism *A. vinosum*. Its precise function could not therefore be conjectured. This protein is predicted to be periplasmic and its gene is located in close vicinity to the *sox* gene cluster, as in some other sulphur oxidizing bacteria, such as *Sulfurimonas* (Suden_0256 and Suden_0267) or *Sulfurovum* (SUN_0493). This suggests the protein is involved in the sulphur transfer during the Sox catalytic cycle. However, it cannot be ruled out that this DsrE-like protein has a functional connection with FccAB (Hhal_1945-1946) whose genes are located inside the same gene cluster. CysB, whose gene is adjacent to a gene coding a sulphur transport domain-containing protein, also more abundant in this condition, is a putative transcriptional regulator of the Cys pathway genes, dedicated to assimilation of sulphur compounds for cysteine synthesis, in which CysH, an adenosine 5-phosphosulphate reductase, is responsible for the production of SO_3^{2-} . The O-acetylhomoserine sulfhydrylase, which reacts with sulphide or other thiols, is known for participating in an alternative pathway of L-homocysteine synthesis (Yamagata, 1989). Proteomic data therefore suggest that, under S^0 , sulphur

compounds assimilation for the cysteine pathway is promoted, at least at specific steps.

The global response of proteins that are predicted to be involved in bioenergetics in *H. halophila* is indicated in Figure S3. Regarding proteins probably involved in sulphur compounds oxidation pathways, the level of the PhsABC enzyme increased significantly in HS^- relative to the two other conditions. The periplasmic Sox system for $S_2O_3^{2-}$ oxidation, seemed to be constitutive, while the Sqr for sulfide oxidation, even if increased in HS^- , does not show significant fold change. No statistically significant difference in protein level could be observed either for the three copies of FccAB, the TusA-like protein (Hhal_1937), a thiol: disulphide interchange protein (Hhal_1944) or proteins with homologies to sulphate transporter (Hhal_1966 and Hhal_1967). However, it is clear that most of the Dsr proteins show a general tendency for an increase in abundance when *H. halophila* grows with HS^- compared to $S_2O_3^{2-}$ (and to a lesser extent to S^0), although these increases were not statistically significant for all of them at the limit of the threshold. Slight changes were also detected for the cytoplasmic sulphite dehydrogenase SoeABC which tends to be in larger amounts with HS^- as an electron donor. Overall, these results indicated that PhsABC, SoeABC and the Dsr system show an increased abundance in cells from HS^- -containing medium and that they are likely regulated according to the reduced sulphur source supplied.

The proteome after growth with thioarsenates (i.e., $HS^- +$ arsenite)

Because *H. halophila* did not grow on arsenite as the sole electron source, we resorted to the comparison of proteomes obtained on HS^- complemented or not with arsenite to reveal proteins that are differentially produced under thioarsenates. The COG enrichment

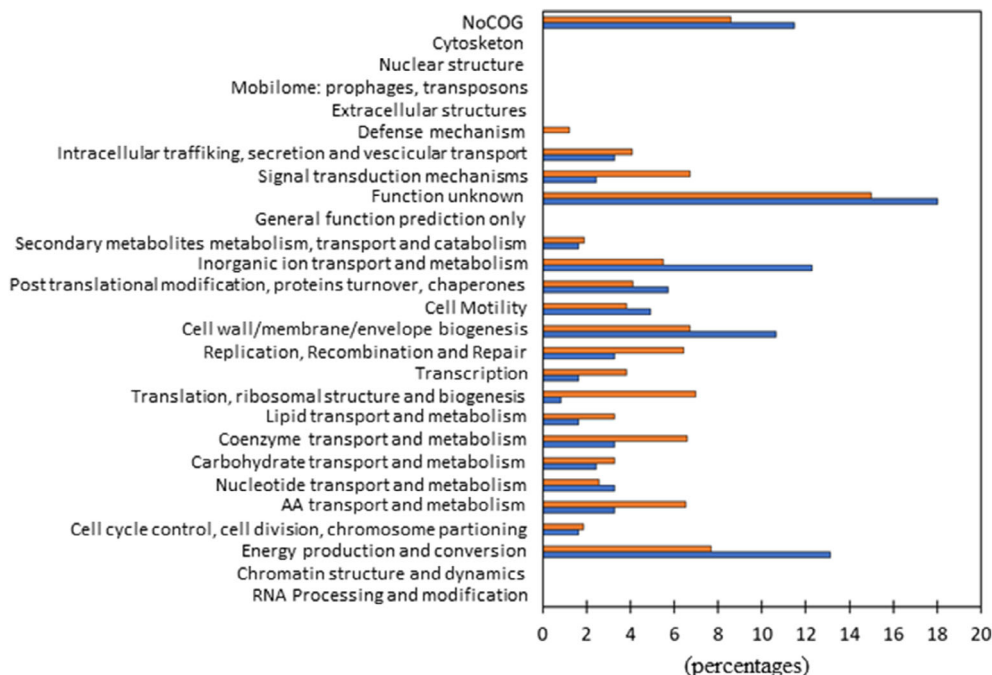


FIGURE 6 COG enrichment analysis of the proteome of *Halorhodospira halophila* under $\text{HS}^- + \text{arsenite}$, compared to HS^- . In orange, % of proteins of the total predicted proteome of *H. halophila* belonging to a specific Cluster. In blue, % of differential proteins (up and down) between $\text{HS}^- + \text{arsenite}$ and HS^- belonging to a specific Cluster.

analysis emphasized that the arsenite affects not only the bioenergetics (Energy production and conversion; Figure 6) of the bacterium but also the inorganic ion transport and metabolism together with the cell wall, membrane and envelope biogenesis (Figure 6). The abundance of 62 and 60 proteins was increased and decreased respectively in cells cultivated with $\text{HS}^- + \text{arsenite}$ compared to HS^- (Figure S9). Among them, proteins of the T6SS (Hhal_0154 to Hhal_0165) and the Pili, which were more abundant in the presence of HS^- compared to other sulphur compounds (Table 2), were also more abundant in HS^- when compared to thioarsenates. The Dsr (Hhal_1951-1963) system, the Phs (Hhal_1164-1166), the Soe (Hhal_1934-1936) and a sulphate transporter (Hhal_1911) were found in statistically significant lower amounts in the presence of thioarsenates (Figure S9, see also Figure S3). These data suggest that several enzyme systems involved in the pathway of HS^- -metabolization are less requested, predominantly those funnelling electrons to the MK pool where cytochrome bc_1 taps into. Regarding proteins produced at higher levels with $\text{HS}^- + \text{arsenite}$ directly related to bioenergetics, we can notice that RnfA-type ion-translocating protein (Hhal_0719) was overproduced together with a Na^+ /solute symporter (Hhal_1899). Both could be involved in the promotion of the Na^+ gradient in this growth condition. The DsrE-like (Hhal_1943), SoxAX and SoxB (Hhal_1948 and Hhal_1939), proteins from the sulphur oxidizing system Sox and one of the three copies of FccB (Hhal_1331), the flavoprotein subunit of the

flavocytochrome c HS^- dehydrogenase, were unexpectedly also overproduced under $\text{HS}^- + \text{arsenite}$ compared to HS^- alone, together with two periplasmic electron carriers, HiPIP III (Hhal_2378) and the cytochrome c_{551}/c_5 (Hhal_0118) (Figure S9). Although HiPIP III is homologous to PioC and might be involved in an electron transfer to/from the extracellular medium via an Mtr/Pio complex, these two soluble electron carriers might well be two electron acceptors (specifically or complementarily) of Sox and Fcc systems, therefore suggesting that the two linear pathways of electron funnelling to the RC (not involving the cytochrome bc_1 complex) are favoured in the presence of $\text{HS}^- + \text{arsenite}$. It should be noted that cytochrome c_{551}/c_5 is the only cytochrome whose level statistically varied in the same way as that of Sox system proteins under all the conditions analysed (i.e., constant level whatever the sulphur compound available and in higher level in $\text{HS}^- + \text{arsenite}$ compared to HS^-).

On the involvement of the cytochrome c_{551}/c_5 and HiPIP III in the photosynthetic electron transfer under thioarsenates

We went further on the hypothesis, raised by proteomic data, of the possible contribution of cytochrome c_{551}/c_5 (Hhal_0118) and HiPIP III (Hhal_2378) to the linear electron supply to the photosynthesis of the strain grown on $\text{HS}^- + \text{arsenite}$ by resorting to functional studies. Both an undetermined cytochrome and HiPIP

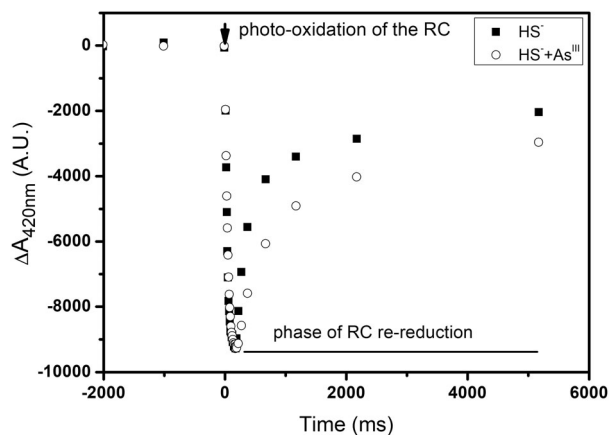


FIGURE 7 Kinetics of flash-induced absorption recorded at 420 nm in whole cells of *Halorhodospira halophila*. Cells were grown either under HS^- (closed squares) or under $\text{HS}^- + \text{As}^{III}$ (open circles). Full oxidation of the RC pool was obtained by constant illumination of the cell suspension before the flash.

It has been previously proposed as electron donors to the tetrahemic cytochrome subunit of the photosynthetic RC based on light-induced absorption spectroscopy on whole cells grown with $\text{S}_2\text{O}_3^{2-} + \text{HS}^-$ (Lieutaud et al., 2005; Menin et al., 1998). Here, we used light-induced absorption on *H. halophila* whole cells to try to determine the contribution of electron carriers in the reduction of RC when HS^- and arsenite are supplied. The distinction between electron transfer from HiPIP or cytochrome towards the tetraheme subunit can be made by tracking at 420 nm the redox state evolution of the RC tetrahemic subunit after its photo-oxidation. In optical spectroscopy, a HiPIP shows a low contribution of oxidized-reduced difference at 420 nm, whereas the contribution of a cytochrome is high. If a cytochrome is the electron donor to the RC tetrahemic subunit, a small variation in the absorption will therefore be observed in the recorded kinetics, after the photo-oxidation, due to absorption compensation between both cytochromes during the RC re-reduction phase. On the other hand, the tetrahemic subunit reduced by a HiPIP will show a strong variation in the light-induced absorption in the RC re-reduction phase. Figure 7 shows kinetics with bacteria grown in the presence of HS^- alone (closed squares) or in the presence of both HS^- and arsenite (open circles). The first phase corresponds to the rapid light-induced oxidation of the RC tetraheme cytochrome, generating a large negative difference of absorption measured against the non-excited reference. The photo-oxidized tetraheme cytochrome returns to the reduced state with a strong variation in absorption suggesting the contribution of a HiPIP to its reduction. The incomplete return to zero suggests that a cytochrome also contributes to the re-reduction of the RC tetraheme subunit in addition to the HiPIP in both growth conditions. The comparison of

the tetraheme cytochrome re-reduction kinetics recorded on bacteria grown in the two conditions suggested that the cytochrome population contribution to this re-reduction is significantly higher in $\text{HS}^- + \text{As}^{III}$.

Because light-induced absorption kinetics on whole cells cannot allow the precise identification of the electron carriers involved in the photosynthesis of *H. halophila*, we purified and characterized the electron carriers and resorted here to experiments with reconstituted systems. We heterologously produced the cytochrome c_{551}/c_5 and HiPIP III in *E. coli* and titrated them at 2.22 M NaCl and pH 8.8 (the physiological conditions of *H. halophila* growth) ($E_m = +77$ mV and $+134$ mV respectively; Table 3). Given the redox potential values for the bacteriochlorophyll special pair, a couple of P^+/P of the RC and the one predicted for the Rieske protein of the cytochrome bc_1 complex (Table 3), the cytochrome c_{551}/c_5 and the HiPIP III seem perfectly suited to reduce the photosynthetic RC and being themselves reduced by the Rieske from the cytochrome bc_1 . These carriers are therefore suited for both a linear (from Sox or Fcc systems) or a cyclic (from the cytochrome bc_1 complex) electron transfer to the photosynthetic RC.

To test the ability of the cytochrome c_{551}/c_5 and HiPIP III to effectively reduce the photo-oxidized photosynthetic RC, we resorted to EPR on purified soluble electron carriers complementing membrane fragments containing RC (Figure 8A,B). HiPIP II has been previously demonstrated to firmly bind to RC. Preparation of membrane fragments by French press preserves this HiPIP II bound to the RC (see Lieutaud et al., 2005) and the EPR signal of HiPIP II (with g_1 at 2.10) was observable in photo-oxidized crude pre-reduced membranes (green spectrum, panel B). Sonication of these crude membranes allows producing membranes devoid of any electron carrier (see Lieutaud et al., 2005). Purified c_{551}/c_5 is EPR silent when reduced but shows a rhombic spectrum with g values at 2.92, 2.29 and 1.43 when chemically oxidized (black spectrum, panel A). Neither illumination of the purified pre-reduced c_{551}/c_5 alone (red spectrum), nor the mixing of this reduced c_{551}/c_5 with sonicated and pre-reduced membranes (purple spectrum), induced oxidation of c_{551}/c_5 . Only the illumination of the sonicated pre-reduced membranes mixed with reduced c_{551}/c_5 did oxidize the latter (blue spectrum), suggesting oxidation of c_{551}/c_5 by photo-oxidized RC for the re-reduction of the latter. An equivalent experiment performed with the HiPIP III suggested that this electron carrier is unable to reduce directly the RC (blue spectrum, Panel B) but could rather participate in its reduction with the HiPIP II as intermediate (orange spectrum). Only when mixed with the crude (containing HiPIP II) pre-reduced membranes and illuminated, HiPIP III, which is EPR silent at the reduced state (purple spectrum), indeed became oxidized (orange spectrum) and then presented (orange

TABLE 3 Redox potential value of photosynthetic components and electron transporters of *H. halophila*.

Protein	Locus tag	E_m , mV	Conditions	Reference
Cytochrome c_{551}/c_5 (native)	nd	+58	0.1 M NaCl and pH 7	Meyer (1985)*
Cytochrome c_{551}/c_5 (recombinant)	Hhal_0118	+77 ± 15	2.22 M NaCl and pH 8.8	This study
P ⁺ /P of the RC**	Hhal_1604-Hhal_1605	+270	2.22 M NaCl and pH 7	Schoepp-Cothenet et al. (2009)
Rieske of the bc_1 complex	Hhal_0182	+120 ± 10	2.22 M NaCl and pH 7	Schoepp-Cothenet et al. (2009)
	Hhal_0182	±60***	2.22 M NaCl and pH 8.8	Extrapolated***
HiPIP III	Hhal_2378	+134 ± 10	2.22 M NaCl and pH 8.8	This study

Abbreviation: nd, not provided.

*Characterized from *H. halophila* BN9626.

**P⁺/P is the bacteriochlorophyll special pair of the RC.

***Taking into account the well-known pH dependence of the Rieske protein's redox potential (see, e.g., Zu et al., 2003).

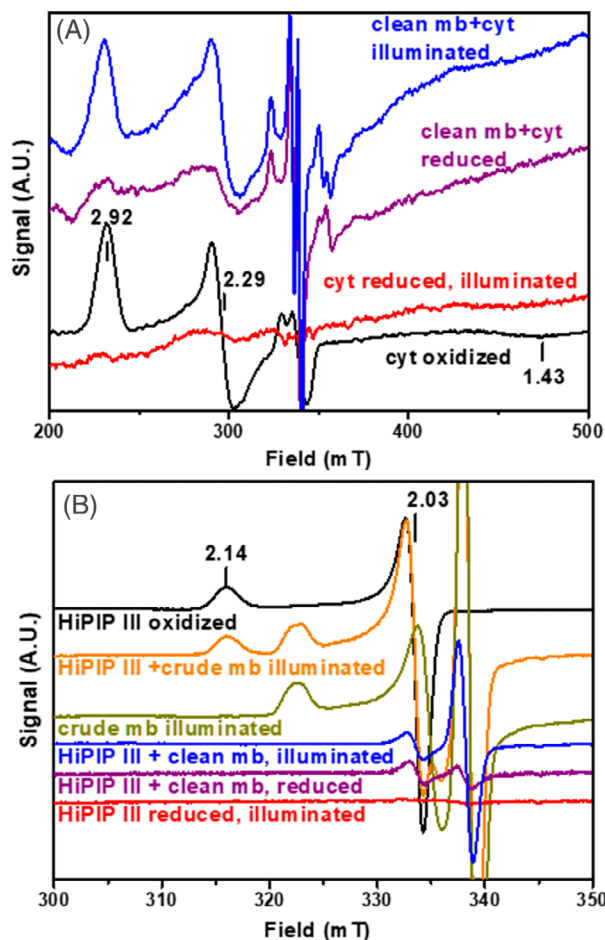


FIGURE 8 Photo-oxidation of cytochrome c_{551}/c_5 (A) and HiPIP III (B) by membranous fragments from *Halorhodospira halophila*. Membranes were prepared from cells grown with HS^- . Black spectra are recorded on chemically oxidized electron carriers. Red spectra are recorded on chemically reduced and subsequently illuminated electron carriers. Purple spectra are recorded on sonicated (clean) and reduced membranes (mb) supplemented with electron carriers. Blue spectra are recorded on the latter samples after illumination. In the case of HiPIP III, illumination experiments were also performed on crude membranes (without sonication), in the absence (green spectrum) or the presence (orange spectrum) of HiPIP III.

spectrum) the characteristic axial spectrum of the chemically oxidized HiPIP III with g values at 2.14 and 2.03 (black spectrum). The EPR data are thus consistent with a possible role for cytochrome c_{551}/c_5 and HiPIP III as electron suppliers to the photosynthetic chain at the RC level.

DISCUSSION

On the proteomic data

DIA-MS and label-free quantification, used in this study, offered high proteomic depth and data completeness. The resulting coverage of the proteome of *H. halophila* is impressive with 88% of the predicted open reading frames identified. Only 299 proteins (listed in Table S4) were not detected in the proteomics dataset. This means that a high proportion of genes are expressed under the four growth conditions tested and that the majority of the bacterium's proteins are maintained in the cell, the regulation being predominantly achieved by varying the level of abundance of proteins in the various environmental conditions. The fact that a significantly lower percentage of proteins (compared to the total proteome) is generally retrieved in previous proteomic studies (e.g., only around 60% of the proteins in the annotated proteome of *E. coli* were found produced under a single condition during exponential growth [Krug et al., 2013]) is considered as a consequence of less performance approach for identification. The high number of common proteins (96%) between the four growth conditions examined might seem also intriguing. It is worth mentioning, however, that the growth conditions differ from each other exclusively by the precise chemical nature of the sulphur compound used as an electron donor to common anaerobic photosynthesis.

It should be pointed out that several membranous proteins theoretically produced under the examined growth conditions were not retrieved, such as PufL (Hhal_1605) and PufM (Hhal_1604) from the



photosynthetic RC (only the tetrahemic subunit, PufC [Hhal_1603] was identified), or NuoJ and K (Hhal_1756 and Hhal_1755; despite all the other subunits of the Complex I was detected). The present applied protocol is however considered not sensitive to the physico-chemical properties of membranous proteins contrary to 2D-electrophoresis (Soufi & Macek, 2015). Indeed, the proteins mentioned above present no evidence that trypsin-generated peptides are not accessible to mass spectrometry. It is therefore highly likely that the main reason for the absence of these proteins is related to their low abundance in the proteomes analysed. Several soluble proteins, for example, FliQ, FliJ, FliE and FliS (Hhal_0483, 0494, 0499, 0503, respectively) from the Fli system (central for export and motility [Macnab, 2004]), MenC (Hhal_1130) from the Men system (for MK biosynthesis [Johnston & Bulloch, 2020]), or the cytochrome subunit (Hhal_1162) of a flavocytochrome *c* sulphide dehydrogenase FccAB, were moreover absent (in one or more growth conditions) whereas the other components of these systems were part of the core proteome. The explanation we propose is that the proteins are missing (see Table S4) either because they are not very abundant in the proteome analysed and/or because they generate peptides that are not accessible to mass spectrometry.

On the sulphur oxidation in *H. halophila*

In *H. halophila*, oxidation of the sulphur source is crucial because the electrons released feed not only the mandatory photosynthetic chain used to generate energy but also biosynthetic processes. We confirmed in the present work that *H. halophila* can grow on sulphide, thiosulphate and commercial S^0 provided extracellularly as a photosynthetic electron donor. Overall, the enzymatic machinery for sulphur compounds oxidation, when the bacterium grows with HS^- or $S_2O_3^{2-}$, resembles the one proposed for other sulphur-oxidizing photosynthetic bacteria. Initiation of oxidation of the reduced substrates via the Sqr and/or the Fcc and the Sox complex takes place in the periplasm and further oxidation of intermediate compounds continues in the cytoplasm with the participation of the reverse Dsr system, producing intracellular SO_3^{2-} , then oxidized by Soe, which releases SO_4^{2-} . Soe appears to be the only enzyme oxidizing SO_3^{2-} , as genes for the adenylsulphate reductase and sat (sulphate adenyltransferase), found in the cytoplasm of *A. vinosum* or *C. tepidum* to convert SO_3^{2-} into SO_4^{2-} , or those for the periplasmic sulphite dehydrogenase Sor have not been identified in the genomic sequence (Frigaard & Dahl, 2009). Sqr, Fcc and Sox appear to be constitutively produced in *H. halophila*, as in *A. vinosum*, but unlike *C. tepidum*, while the Dsr system, and to a less extent Soe, are specifically increased in HS^- , i.e. when

sulphur is stored in globules as intermediate. The reverse Dsr is known to be required for oxidation of stored sulphur in bacteria (Holkenbrink et al., 2011; Pott & Dahl, 1998).

Proteomic data showed a statistically significant higher production of Phs in the HS^- condition, suggesting this putative enzyme to be specifically involved in the overall HS^- oxidation pathway (Table 1; Figures S5 and S6). The function of Phs, described to convert $S_2O_3^{2-}$ into SO_3^{2-} and HS^- , is puzzling in the scheme of the use of sulphur compounds in *H. halophila*. A putative reverse functioning of this enzyme as HS^- oxidase (which is thermodynamically favourable and reported in *Salmonella enterica* [Stoffels et al., 2012]) is not favoured here because HS^- is completely exhausted after 15 h of *H. halophila* growth (Figure 2C), that is, well before the end of the exponential phase, a time point at which cells were harvested for proteomic analysis. We propose instead that PhsABC may eventually participate in the mobilization of solid extracellular sulphur deposited during growth on HS^- , by releasing SO_3^{2-} in the periplasm from $S_2O_3^{2-}$ which would be available in small amounts in the growth medium under this condition. The water-soluble SO_3^{2-} could be released extracellularly to chemically react with sulphur, producing $S_2O_3^{2-}$ that could re-enter and be used by cells as proposed for *S. enterica* or *Shewanella oneidensis* (Burns & DiChristina, 2009; Hinsley & Berks, 2002). Interestingly, this Phs enzyme belongs to the large molybdoenzyme family including the periplasmic Psr/Sre. In *A. vinosum* and *C. tepidum*, genes for an enzyme annotated as Psr/SreABC (sulphur/polysulphide reductase) showed an increased expression in HS^- medium and a potential role for this enzyme in the oxidation of polysulphide (formed from HS^-) into stored sulphur and thus in globules formation was put forward (Eddie & Hanson, 2013; Weissgerber et al., 2014).

The growth of *H. halophila* on exogenous S^0 is puzzling. The fact that the electron source was not oxidized up to SO_4^{2-} (nor $S_2O_3^{2-}$ or SO_3^{2-}) indicates that the bacteria may oxidize commercial sulphur and deposit biogenic sulphur globules that would not be degraded under the growth conditions used in this study, as previously shown for various *Halorhodospira* species (Franz et al., 2009). It is currently unknown whether the sulphur stored in globules after growth on chemical S^0 constitutes a form of sulphur that can be used and oxidized by cells under certain conditions. It should be pointed out, however, that the excess of S^0 , used here (62.5 mM) and in the study of Franz et al. (2009; 50 mM), which may explain the lack of remobilisation of sulphur stored in globules and the preference for the bacteria to use commercial S^0 as long as it is available. The phase-contrast microscopy suggests that in this condition, the sulphur globules could be inside the cells (Figure 2F). Additional experiments are underway to



confirm this observation which would make *H. halophila* the second strain described for its ability to form both external and internal sulphur globules (see Bryantseva et al., 1999). It is to be noted that the presence of such unusual (internal or sticking) sulphur globules still at the end of growth would explain the concomitant absence of SO_4^{2-} detection and lower expression of T6SS and Pili under S^0 compared to HS^- . Proteomics analyses have already proposed that Pili proteins are involved in cell motility and adhesion to globules (Florentino et al., 2019). Such movements of cells towards globules have been observed in *C. tepidum* (Marnocha et al., 2016). T6SS proteins could be involved in the formation and/or mobilization of globules. Recent work on an *H. halophila*-related species, *Thioalkalivibrio versutus*, an *Ectothiorhodospiraceae*, established that the external sulphur globules are wrapped within an organic layer composed of polysaccharides and proteins (Liu et al., 2022), in a similar fashion than in other sulphur-oxidizing species belonging to the *Chlorobiaceae* and *Chromatiaceae* families (Frigaard & Dahl, 2009; Marnocha et al., 2019). However, the involved proteins are unknown but different from the Sgp ones, identified in *A. vinosum*. In *C. tepidum*, the formation and degradation of external sulphur globules have been shown to process also at a distance from the cells (Marnocha et al., 2016).

On the photosynthetic transporters and reducing power synthesis/consumption

Whatever the sulphur compounds, the electrons coming from their oxidation are potentially delivered into the photosynthetic chain. We identified eight periplasmic electron carriers from the genomic sequence of *H. halophila*, five of which are present in the four growth conditions analysed, at unequal approximate abundance in the cell (Figure S3; Table S5). The multiplicity of electron shuttles in bacterial photosynthesis is common allowing either adaptation to various ambient redox potentials and growth conditions or complementarity between linear and cyclic electron transfers to the RC (Bird et al., 2014; Menin et al., 1997; Ohmine et al., 2009). In the case of *R. gelatinosus*, up to four electron donors to the RC have been demonstrated, for example, two isoforms of cytochrome c_8 , one cytochrome c_4 and one HiPIP (Ohmine et al., 2009). This also seems to be the case in *H. halophila*. The well-characterized (in *H. halophila* BN9626) HiPIP I (Hhal_1488 in *H. halophila* SL1) was not found in the whole-cell proteomic analysis and therefore cannot be attributed to specific growth conditions (Table S5). HiPIP II has previously been demonstrated to be an efficient electron donor to RC under sulphide conditions (Lieutaud et al., 2005) and the present proteomic data revealed that it is not produced in the presence of

$\text{S}_2\text{O}_3^{2-}$ alone (Figure S3). Its redox potential makes it compatible with either linear or cyclic photosynthetic electron transfer in sulphide conditions. This proteomic work is the first to reveal the production of HiPIP IV in *H. halophila* (whatever the electron donor; Figure S3). The proximity of the gene encoding this HiPIP to those of a large photosynthetic gene cluster (*hhal_1625-hhal_1637*) suggests a function for HiPIP IV in photosynthesis. In the present work, we have proposed HiPIP III and cytochrome c_{551}/c_5 as potential additional photosynthetic electron carriers (see below). Proteomics suggest that production of these electron transporters is specifically increased under thioarsenates condition (Figures S3 and S9), with HiPIP III potentially acting in coordination with HiPIP II in these conditions. It should be noted that the regulation of HiPIP II and HiPIP III production follows the same trend (Figure S3). The involvement of cytochrome c_{551}/c_5 , homologous to *Chlorobiaceae* c_5 , in photosynthesis in *H. halophila* would be similar to the proposed participation of c_5 in photosynthetic cyclic electron transfer between the RC and the cytochrome bc_1 complex (Imhoff et al., 2022).

The proteomic analysis detects Complex I in all the growth conditions examined, which reinforces the model that *H. halophila*, in the same way as other PSB, uses Complex I for reverse electron flow to produce reducing power (NADH) from oxidation of quinones. In addition, two putative NAD^+/NADH oxidoreductases Rnf-Nqr-Rsx complexes (Hhal_0061-0067 and Hhal_0719-0723) are produced (Figure 5; Figure S3). The presence, close to Hhal_0061-0067, of genes homologous to *iorA* (Hhal_0068), *iorB* (Hhal_0069) and a phenylacetate-CoA ligase gene (Hhal_0070) suggests this cluster to code for a complex involved in NADH oxidation for the reduction of a low-redox potential ferredoxin (at the expense of the ion gradient) needed for amino-acids biosynthesis by the indole-pyruvate oxidoreductase IOR as described for other micro-organisms (Porat et al., 2004). The second gene cluster is immediately upstream of an endonuclease *nth*-homologue gene (*hhal_0724*), as already observed in various bacteria, *nth* being co-transcribed with *rsx* genes in *E. coli* (Gifford & Wallace, 2000). No clue allows us to predict the directionality of this complex's reaction. A third Rnf-type complex (Hhal_0283-0289), probably reducing a low-redox potential ferredoxin used for nitrogen fixation, is not identified in all the growth conditions, unlike the two other complexes. For all these Rnf-type complexes, the question also arises about the ion gradient used for their function: H^+ or Na^+ . It would be tempting to propose the Na^+ gradient to be used (in addition to the H^+ one) since *H. halophila* grows at pH 8.8. Moreover, Dsr (via DsrL), has been proposed for producing NAD(P)H (Löffler et al., 2020). This complex could therefore contribute to the generation of reducing power also in *H. halophila* (Figure 5).



On the disability of *H. halophila* to grow on arsenite alone

An intriguing feature of the Arx enzyme is its constitutive production in *H. halophila*, although the strain is unable to grow on arsenite alone. The expression of genes encoding this enzyme is described as being regulated by arsenite in other bacteria (Durante-Rodríguez et al., 2019; Hernandez-Maldonado et al., 2017; Zargar et al., 2012). Examination of the *H. halophila* *arx* cluster (Figure S2B) revealed that it does not contain genes for the regulatory elements (*arxRSX*) unlike most other bacteria carrying the cluster (Durante-Rodríguez et al., 2019; Hernandez-Maldonado et al., 2017; Zargar et al., 2012). The lack of the regulatory elements in *H. halophila* could not explain the inability of this bacterium to grow on arsenite alone, since Arx is observed in all the growth conditions. *Ectothiorhodospira* (*E.*) *shaposhnikovii*, which does contain these genes (data not shown), is also unable to grow on arsenite alone (Hoeft McCann et al., 2016).

The fact that Arx reduces the UQ pool only (Szyttenholm et al., 2020), while the photosynthetic cyclic electron flow uses the MK in *H. halophila* (Schoepp-Cothenet et al., 2009) could be put forward for an inefficient oxidation of arsenite for photosynthesis in this strain under the anaerobic conditions examined. As stated above, the presence of Ubi proteins dedicated to both O₂-independent and O₂-dependent UQ biosynthesis, in the proteome in all the four growth conditions analysed, confirmed that *H. halophila* is enzymatically equipped to produce UQ (a high redox potential quinone) in anaerobiosis. This allows Arx (see Szyttenholm et al., 2020) to work anaerobically. It is to be noted that the overall trend of Ubi and Men enzymes observed in the proteomic analysis (Figure S3) is perfectly in line with the relative enrichment of UQ compared to MK in the presence of As together with HS⁻ (Szyttenholm et al., 2020).

The *bc*₁ complex could also be put forward to explain the inefficient connection of arsenite oxidation with photosynthesis. The Rieske protein sequence analysis of *E. shaposhnikovii* (with S and F residues characteristic of high redox potential Rieske; see ten Brink et al., 2013 and references herein) suggests that the cytochrome *bc*₁ complex of this bacterium uses UQ, similar to the ones of *Ectothiorhodospira* sp. BSL-9 and PHS-1 (Figure S10), implying that the cyclic electron flow uses the UQ pool in all three bacteria, as established in *A. vinosum* (Dutton & Leigh, 1973; Halsey & Parson, 1974). Only *Ectothiorhodospira* sp. BSL-9 and PHS-1 are, however, proposed to be able to grow on arsenite alone (Hoeft McCann et al., 2016), suggesting that the nature of the Q-pool used in the photosynthetic machinery in these bacteria is also not the explanation for the capability or not to grow on this substrate. The reason for the lack of

growth of *H. halophila* and *E. shaposhnikovii* on arsenite is furthermore not related to the *ars* genes (involved in arsenic resistance) since the *ars* gene repertoire of *E. shaposhnikovii* is strictly identical to the one of *Ectothiorhodospira* sp. BSL-9 and PHS-1. Some putative *ars* genes are also present in *H. halophila* genome: *arsA* (*hhal_2193*), *arsB* (*hhal_0309*) and *arsC* (*hhal_0091*). *ArsA* and *ArsB* are respectively constitutive and induced by arsenite in *H. halophila* (not shown) and should therefore allow the bacterial resistance to this toxic compound. The explanation of the absence of growth of the strain under arsenite is thus not straightforward and this needs to be further investigated, including characterizing the Arx system.

The second intriguing feature of Arx is the presence of two genes coding for two Fe-S subunits, ArxB' and ArxB (*Hhal_0352* and *Hhal_0354*; Figure S2B) instead of only the one present in the sister enzyme Arr. Both ArxB proteins are identified in *H. halophila* by our proteomic analysis, as previously observed in *E. sp.* BSL-9 (Hernandez-Maldonado et al., 2017). It is not established whether each of the ArxB subunits is part of a specific Arx complex version or if they are both part of the same complex as proposed by (Hernandez-Maldonado et al., 2017). It should be noted, however, that ArxB' is largely under-represented relatively to ArxB (although of a similar chemical nature), in samples from all conditions analysed by proteomics (Table S3). We furthermore do not detect ArxB' (only ArxA and ArxB) in the band showing arsenate reductase activity in gel (data not shown). These data do not support the proposed idea (see Hernandez-Maldonado et al., 2017) that both ArxB and ArxB' are part of the same complex.

The fact that *H. halophila* does not grow on arsenite alone does not prevent it from converting arsenite to the less toxic form of arsenate for detoxification. Electrons coming from the turnover of Arx, feeding the UQ pool could serve for UQ oxidizing enzymes such as the *bd* oxidase, but the energy generated seems insufficient to grow once the energy required to fight arsenic toxicity has been consumed.

On the pathway of thioarsenates cycling

Our comparative quantitative proteomics study established that the production of several proteins known to be involved in sulphur metabolism is impacted (positively or negatively) when arsenite is added to HS⁻. Dsr proteins, Soe and Phs enzymes, and a SO₄²⁻ transporter are lowered, while both one Fcc (there are three copies in *H. halophila*) and the Sox pathway (enzymes and possible electron carriers) are promoted in the presence of arsenite and HS⁻ in comparison to HS⁻ alone. The sole comparable study analysing the impact of the addition of arsenite to a sulphur compound is a



transcriptomic analysis of *Thioalkalivibrio* species where arsenite has been added to $S_2O_3^{2-}$ (Ahn et al., 2019). It diverges from our results for Soe and Dsr while converging with our results on the Na^+/H^+ transporter or DsrE. The simple fact that we used, in our study, proteomics instead of a transcriptomic approach and HS^- instead of $S_2O_3^{2-}$, could explain this divergence.

In our study, performed in the presence of HS^- + arsenite, thioarsenate species have been revealed. Quantification of thioarsenate indicated that relatively small amounts are produced from the chemical reaction between HS^- and arsenite (Figure 3F) and that biotic activity is required to generate more significant amounts of thioarsenate and also to consume them. This has been previously proposed to be due to bacterial HS^- oxidation, forming polysulphide, and subsequent reaction of this S(0) with arsenite. As trithioarsenate, which requires a S(-II) sulphur species for its formation, is the predominant species observed (Figure 3E), HS^- could also be involved. Quantification of HS^- in biotic experiments (growth on sole HS^- ; Figure 2) suggests that HS^- is exhausted within the first 15 h of bacterial growth (in contrast to what is observed in abiotic controls) and this corresponds more or less to the time range of formation of thioarsenates (Figure 3E). Kinetic of HS^- conversion specifically in the presence of arsenite has however to be confirmed. It is to be noted that it is the arsenite (not arsenate eventually produced here by the Arx) that has been proposed to react to form thioarsenate (Planer-Friedrich et al., 2015). The generated thioarsenate is then consumed by bacteria to form the end products arsenate

and SO_4^{2-} . The kinetics suggest not only that these two end products are produced at a common step (see Figure 3C,D) but also that this step is the main one enabling growth (see Figure 3 panel A compared with panel E). Our results therefore suggest that it is a specific metabolic pathway for thioarsenate conversion that is highlighted here. While the Fcc enzyme has been established to be strictly specific towards HS^- , and does not accommodate other sulphur compounds such as $S_2O_3^{2-}$, S^0 or $S_4O_6^{2-}$ (Tikhonova et al., 2021), Sox shows a broader substrate spectrum. Based on the chemical similarity between thioarsenate and $S_2O_3^{2-}$, Sox had been discussed in the past as a possible enzyme responsible for thioarsenate conversion (Edwardson et al., 2014). Recent analysis of correlations between environmental factors and microbial functional genes reinforced this proposition (Qing et al., 2023). As outlined above, a transcriptomic analysis of *Thioalkalivibrio* species analysed the impact of arsenite addition to sulphur compound. Sox involvement in the conversion of a hypothetically formed thioarsenate has also been proposed but the data are ambiguous, with *Tv. Thiocyanoxidans* ARh2^T shows an upregulation of sox genes in the presence of $S_2O_3^{2-}$ + arsenite compared with $S_2O_3^{2-}$ alone, while *Tv. jannischii* ALM2^T shows the opposite (Ahn et al., 2019). The present proteomic analysis goes further in the hypothesis of Sox involvement in thioarsenate conversion. A mechanism of thioarsenate conversion by Sox would be very close to the one proposed for $S_2O_3^{2-}$ (Figure 9A,B). We present a model for monothioarsenate but the model is suitable for any thioarsenate form. In this model, the monothioarsenate

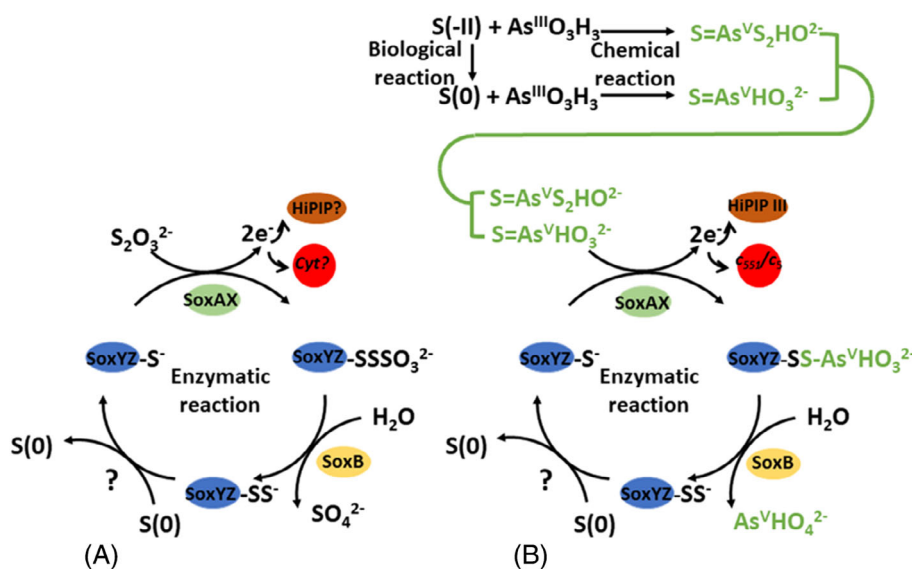


FIGURE 9 Model for $S_2O_3^{2-}$ (A) or thioarsenate (B) oxidation by the Sox system. The $S_2O_3^{2-}$ oxidation pathway was proposed by Frigaard and Dahl (2009). The exact form of S(0) released from SoxYZ is unknown. S(0) reacting with arsenite was proposed to be polysulphide (Planer-Friedrich et al., 2015). $As^{III}O_3H_3$, $S=As^V S_2HO_2^{2-}$, $S=As^V HO_3^{2-}$ and $As^V HO_4^{2-}$ correspond to arsenite, trithioarsenate, monothioarsenate and arsenate, respectively.



would be bound to the reactive cysteine of SoxYZ by its sulphur atom similarly to $S_2O_3^{2-}$. SoxB would release arsenate and the cycle would then proceed as usually described with the formation of a sulphur intermediate. In contrast to the oxidation of $S_2O_3^{2-}$, no SO_4^{2-} would be released by Sox in this case.

We therefore propose that under $HS^- +$ arsenite, Fcc and Sqr would participate in the oxidation of the excess of HS^- to promote the linear and cyclic electron transfer to RC, respectively, while Sox would convert the chemically formed thioarsenate compound to release the first final product arsenate and an intermediate sulphur compound S(0), which would be further metabolized up to SO_4^{2-} by the sulphur compounds oxidizing enzymes. It is to be noted that because arsenate reductase activity is observed on membrane fragments containing Arx (see Figure S2) we can consider the participation of Arx in partial oxidation of arsenite under $HS^- +$ arsenite. The involvement of Sox in the conversion of thioarsenate requires experimental validation and a more in-depth characterization of this enzymatic system. In our model, Fcc and Sox would promote the periplasmic linear electron transfer to the RC, with the possible involvement of the carriers HiPIP III and cytochrome c_{551}/c_5 that would accept electrons from these enzymes and participate in the reduction of the photo-oxidized RC, as we have shown by EPR. The role of c_{551}/c_5 in *H. halophila* SL1 would be therefore equivalent to the one of the c_{554}/c_{555} between the Sox system and the RC in *Chlorobium limicola* (Azai et al., 2010) when oxidizing reduced sulphur compounds.

CONCLUSION

A comparative proteomic analysis was conducted here on an anaerobic photosynthetic bacterium living in hypersaline and alkaline environments, with sulphur and arsenic as electron donors for their photosynthesis and reducing power. This study, the first to our knowledge to be carried out at the protein level, has provided a detailed metabolic reconstruction of *H. halophila*. In this bacterium, the production of enzymes involved in the oxidative metabolism of sulphur compounds appears to be weakly regulated overall. Levels of Phs, as well as proteins building up the T6SS, in cells from different media, suggest that these two systems play a key role in the sulphide oxidation pathway and potentially in the formation and/or degradation of sulphur globules. The arsenite oxidase Arx is constitutive and does not allow the growth of *H. halophila* on sole arsenite. The present study represents also an important step in understanding the use of thioarsenate species as electron donors for bioenergetic purposes by prokaryotes. Thioarsenates, whose determination is very challenging, have received little attention despite their

importance and prevalence in certain arsenic-contaminated environments. In particular, their use and transformation by bacteria are still completely unknown. In cultures of *H. halophila* grown with thioarsenates, the higher abundance of proteins of the Sox system suggests the involvement of this periplasmic thiosulphate-oxidizing enzyme system in thioarsenates metabolism. Proteomic and biochemical data further indicate that cytochrome c_{551}/c_5 and the HiPIP III may transport electrons from Sox to the photosynthetic RC. A function of the Sox system in the metabolism of thiolated arsenic compounds would further strengthen the repeatedly reported interplay between the sulphur and arsenic cycles (D'Ermo et al., 2024). This additional role of the Sox system needs to be confirmed by further analyses but the present data are the first tangible explanation of the metabolism of thioarsenate.

AUTHOR CONTRIBUTIONS

Giulia D'Ermo: Investigation; formal analysis; writing – review and editing. **Stéphane Audebert:** Investigation; formal analysis; writing – review and editing. **Luc Camoin:** Investigation; formal analysis; writing – review and editing. **Britta Planer-Friedrich:** Investigation; writing – review and editing. **Corinne Casiot-Marouani:** Investigation; formal analysis; writing – review and editing. **Sophie Delpoux:** Investigation; formal analysis. **Régine Lebrun:** Investigation; formal analysis; writing – review and editing. **Marianne Guiral:** Conceptualization; investigation; methodology; formal analysis; writing – review and editing. **Barbara Schoepp-Cothenet:** Conceptualization; investigation; methodology; formal analysis; writing – review and editing.

ACKNOWLEDGEMENTS

The authors gratefully acknowledge Sylvia Hafner (BAYCEER, University of Bayreuth) for IC-ICP-MS analysis and raw data interpretation and Julián Bulssico (LCB, Marseille) for Phase-contrast microscopy analysis. The Marseille Proteomics (MaP; marseille-proteomique.univ-amu.fr) platform is supported by Institut Paoli-Calmettes, Centre de Recherche en Cancérologie de Marseille, IBISA (Infrastructures Biologie Santé et Agronomie), the Cancéropôle PACA, FEDER projet Fight Cancer, the Provence-Alpes-Côte d'Azur Région, and Aix-Marseille University. G. D'Ermo's thesis was co-funded by the Région Provence-Alpes-Côte d'Azur and the company GERME S.A. (Marseille).

CONFLICT OF INTEREST STATEMENT

The authors declare no conflicts of interest.

DATA AVAILABILITY STATEMENT

The data that support the findings of this study are openly available in Proteomexchange: <https://proteomecentral.proteomexchange.org/cgi/GetDataset?ID=PXD049262>.



ORCID

Barbara Schoepp-Cothenet  <https://orcid.org/0000-0002-6820-4478>

REFERENCES

- Ahn, A.C., Cavalca, L., Colombo, M., Schuurmans, J.M., Sorokin, D.Y. & Muyzer, G. (2019) Transcriptomic analysis of two Thioalkalivibrio species under arsenite stress revealed a potential candidate gene for an alternative arsenite oxidation pathway. *Frontiers in Microbiology*, 10, 1514.
- Arslan, E., Schulz, H., Zufferey, R., Kunzler, P. & Thony-Meyer, L. (1998) Overproduction of the Bradyrhizobium japonicum c-type cytochrome subunits of the cbb3 oxidase in *Escherichia coli*. *Biochemical and Biophysical Research Communications*, 251, 744–747.
- Azai, C., Tsukatani, Y., Itoh, S. & Oh-oka, H. (2010) C-type cytochromes in the photosynthetic electron transfer pathways in green sulfur bacteria and heliobacteria. *Photosynthesis Research*, 104, 189–199.
- Beard, S., Paradela, A., Albar, J.P. & Jerez, C.A. (2011) Growth of *Acidithiobacillus Ferrooxidans* ATCC 23270 in thiosulfate under oxygen-limiting conditions generates extracellular sulfur globules by means of a secreted tetrathionate hydrolase. *Frontiers in Microbiology*, 2, 79.
- Ben Fekih, I., Zhang, C., Li, Y.P., Zhao, Y., Alwathnani, H.A., Saquib, Q. et al. (2018) Distribution of arsenic resistance genes in prokaryotes. *Frontiers in Microbiology*, 9, 2473.
- Bersch, B., Blackledge, M.J., Meyer, T.E. & Marion, D. (1996) Ectothiorhodospira halophila ferrocyclochrome c551: solution structure and comparison with bacterial cytochromes c. *Journal of Molecular Biology*, 264, 567–584.
- Bird, L.J., Saraiva, I.H., Park, S., Calcada, E.O., Salgueiro, C.A., Nitschke, W. et al. (2014) Nonredundant roles for cytochrome c2 and two high-potential iron-sulfur proteins in the photoferrotothroph Rhodospseudomonas palustris TIE-1. *Journal of Bacteriology*, 196, 850–858.
- Boughanemi, S., Infossi, P., Giudici-Ortoni, M.T., Schoepp-Cothenet, B. & Guiral, M. (2020) Sulfite oxidation by the quinone-reducing molybdenum sulfite dehydrogenase SoeABC from the bacterium Aquifex aeolicus. *Biochimica et Biophysica Acta*, 1861, 148279.
- Brönstrup, M. (2004) Absolute quantification strategies in proteomics based on mass spectrometry. *Expert Review of Proteomics*, 1, 503–512.
- Bryantseva, I., Gorkenko, V.M., Kompantseva, E.I., Imhoff, J.F., Suling, J. & Mityushina, L. (1999) Thiorhodospira sibirica gen. nov., sp. nov., a new alkaliphilic purple sulfur bacterium from a Siberian soda lake. *International Journal of Systematic Bacteriology*, 49(Pt 2), 697–703.
- Budinoff, C.R. & Hollibaugh, J.T. (2008) Arsenite-dependent photoautotrophy by an Ectothiorhodospira-dominated consortium. *ISME Journal*, 2, 340–343.
- Burns, J.L. & DiChristina, T.J. (2009) Anaerobic respiration of elemental sulfur and thiosulfate by Shewanella oneidensis MR-1 requires psrA, a homolog of the phsA gene of Salmonella enterica serovar typhimurium LT2. *Applied Environmental Microbiology*, 75, 5209–5217.
- Challacombe, J.F., Majid, S., Deole, R., Brettin, T.S., Bruce, D., Delano, S.F. et al. (2013) Complete genome sequence of Halorhodospira halophila SL1. *Standards in Genomic Sciences*, 8, 206–214.
- D'Ermo, G., Guiral, M. & Schoepp-Cothenet, B. (2024) The complex interplay of sulfur and arsenic bioenergetic metabolisms in the arsenic geochemical. In: Staicu, L.C. & Barton, L.L. (Eds.) *Geomicrobiology: natural and anthropogenic settings*. Cham, Switzerland: Springer Nature Switzerland AG. ISBN 978-3-031-54305-0.
- Durante-Rodríguez, G., Fernández-Llamas, H., Alonso-Fernandes, E., Fernández-Muñiz, M.N., Muñoz-Olivas, R., Díaz, E. et al. (2019) ArxA from Azoarcus sp. CIB, an anaerobic arsenite oxidase from an obligate heterotrophic and mesophilic bacterium. *Frontiers in Microbiology*, 10, 1699.
- Dutton, P.L. (1971) Oxidation-reduction potential dependence of the interaction of cytochromes, bacteriochlorophyll and carotenoids at 77 degrees K in chromatophores of Chromatium D and Rhodospseudomonas gelatinosa. *Biochimica et Biophysica Acta*, 226, 63–80.
- Dutton, P.L. & Leigh, J.S. (1973) Electron spin resonance characterization of Chromatium D hemes, non-heme irons and the components involved in primary photochemistry. *Biochimica et Biophysica Acta*, 314, 178–190.
- Eddie, B.J. & Hanson, T.E. (2013) Chlorobaculum tepidum TLS displays a complex transcriptional response to sulfide addition. *Journal of Bacteriology*, 195, 399–408.
- Edwardson, C.F., Planer-Friedrich, B. & Hollibaugh, J.T. (2014) Transformation of monothioarsenate by haloalkaliphilic, anoxygenic photosynthetic purple sulfur bacteria. *FEMS Microbiology Ecology*, 90, 858–868.
- Florentino, A.P., Pereira, I.A.C., Boeren, S., van den Born, M., Stams, A.J.M. & Sanchez-Andrea, I. (2019) Insight into the sulfur metabolism of Desulfurella amilii by differential proteomics. *Environmental Microbiology*, 21, 209–225.
- Frankenfield, A.M., Ni, J., Ahmed, M. & Hao, L. (2022) Protein contaminants matter: building universal protein contaminant libraries for DDA and DIA proteomics. *Journal of Proteome Research*, 21, 2104–2113.
- Franz, B., Lichtenberg, H., Dahl, C., Hormes, J. & Prange, A. (2009) Utilization of “elemental” sulfur by different phototrophic sulfur bacteria (Chromatiaceae, Ectothiorhodospiraceae): a sulfur K-edge XANES spectroscopy study. *Journal of Physics: Conference Series*, 190, 5.
- Frigaard, N.-U. & Dahl, C. (2009) Sulfur metabolism in phototrophic sulfur bacteria. *Advances in Microbial Physiology*, 54, 105–179.
- Gerault, M.A., Camoin, L. & Granjeaud, S. (2024) DIAGui: a shiny application to process the output from DIA-NN. *Bioinformatics Advances*, 4, vbae001.
- Gifford, C.M. & Wallace, S.S. (2000) The genes encoding endonuclease VIII and endonuclease III in *Escherichia coli* are transcribed as the terminal genes in operons. *Nucleic Acids Research*, 28, 762–769.
- Gillet, L.C., Navarro, P., Tate, S., Rost, H., Selevsek, N., Reiter, L. et al. (2012) Targeted data extraction of the MS/MS spectra generated by data-independent acquisition: a new concept for consistent and accurate proteome analysis. *Molecular and Cellular Proteomics*, 11(6), O111.016717.
- Halsey, Y.D. & Parson, W.W. (1974) Identification of ubiquinone as the secondary electron acceptor in the photosynthetic apparatus of Chromatium vinosum. *Biochimica et Biophysica Acta*, 347, 404–416.
- Hartig, C., Lohmayer, R., Kolb, S., Horn, M.A., Inskeep, W.P. & Planer-Friedrich, B. (2014) Chemolithotrophic growth of the aerobic hyperthermophilic bacterium Thermocrinis ruber OC 14/7/2 on monothioarsenate and arsenite. *FEMS Microbiology Ecology*, 90, 747–760.
- Hernandez-Maldonado, J., Sanchez-Sedillo, B., Stoneburner, B., Boren, A., Miller, L., McCann, S. et al. (2017) The genetic basis of anoxygenic photosynthetic arsenite oxidation. *Environmental Microbiology*, 19, 130–141.
- Hinsley, A.P. & Berks, B.C. (2002) Specificity of respiratory pathways involved in the reduction of sulfur compounds by Salmonella enterica. *Microbiology*, 148, 3631–3638.
- Hoeltl, McCann, S., Boren, A., Hernandez-Maldonado, J., Stoneburner, B., Saltikov, C.W., Stolz, J.F. et al. (2016) Arsenite as an electron donor for anoxygenic photosynthesis: description



- of three strains of *Ectothiorhodospira* from Mono Lake, California and Big Soda Lake, Nevada. *Life*, 7, 1.
- Holkenbrink, C., Barbas, S.O., Mellerup, A., Otaki, H. & Frigaard, N.U. (2011) Sulfur globule oxidation in green sulfur bacteria is dependent on the dissimilatory sulfite reductase system. *Microbiology (Reading)*, 157, 1229–1239.
- Imhoff, J.F., Kyndt, J.A. & Meyer, T.E. (2022) Genomic comparison, phylogeny and taxonomic reevaluation of the Ectothiorhodospiraceae and description of *Halorhodospiraceae* fam. nov. and *Halochlorospira* gen. nov. *Microorganisms*, 10(2), 295.
- Johnston, J.M. & Bulloch, E.M. (2020) Advances in menaquinone biosynthesis: sublocalisation and allosteric regulation. *Current Opinion in Structural Biology*, 65, 33–41.
- Joliot, P., Béal, D. & Frilley, B. (1980) A new spectrophotometric method aimed at studying photosynthetic reactions. *Journal de Chimie Physique*, 77, 8.
- Krug, K., Carpy, A., Behrends, G., Matic, K. & Soares, N.C. (2013) Deep coverage of the *Escherichia coli* proteome enables the assessment of false discovery rates in simple proteogenomic experiments. *Molecular and Cellular Proteomics*, 12(11), 3420–3430.
- Kulp, T.R., Hoefft, S.E., Asao, M., Madigan, M.T., Hollibaugh, J.T., Fisher, J.C. et al. (2008) Arsenic(III) fuels anoxygenic photosynthesis in hot spring biofilms from Mono Lake, California. *Science*, 321, 967–970.
- Kumari, N. & Jagadevan, S. (2016) Genetic identification of arsenate reductase and arsenite oxidase in redox transformations carried out by arsenic metabolising prokaryotes – a comprehensive review. *Chemosphere*, 163, 400–412.
- Kushkevych, I., Prochazka, J., Gajdacs, M., Rittmann, S.K.R. & Vitezova, M. (2021) Molecular physiology of anaerobic phototrophic purple and green sulfur bacteria. *International Journal of Molecular Science*, 22(12), 6398.
- Lieutaud, C., Alric, J., Bauzan, M., Nitschke, W. & Schoepp-Cothenet, B. (2005) Study of the high-potential iron sulfur protein in *Halorhodospira halophila* confirms that it is distinct from cytochrome c as electron carrier. *Proceedings. National Academy of Sciences. United States of America*, 102, 3260–3265.
- Liu, Z., Yang, M., Mu, T., Liu, J., Chen, L., Miao, D. et al. (2022) Organic layer characteristics and microbial utilization of the bio-sulfur globules produced by haloalkaliphilic *Thioalkalivibrio versutus* D301 during biological desulfurization. *Extremophiles*, 26, 27.
- Löffler, M., Wallerang, K.B., Venceslau, S.S., Pereira, I.A.C. & Dahl, C. (2020) The iron-sulfur Flavoprotein DsrL as NAD(P)H: acceptor oxidoreductase in oxidative and reductive dissimilatory sulfur metabolism. *Frontiers in Microbiology*, 11, 578209.
- Ludwig, C., Gillet, L., Rosenberger, G., Amon, S., Collins, B.C. & Aebersold, R. (2018) Data-independent acquisition-based SWATH-MS for quantitative proteomics: a tutorial. *Molecular Systems of Biology*, 14, e8126.
- Macnab, R.M. (2004) Type III flagellar protein export and flagellar assembly. *Biochimica et Biophysica Acta*, 1694, 207–217.
- Mamocho, C.L., Levy, A.T., Powell, D.H., Hanson, T.E. & Chan, C.S. (2016) Mechanisms of extracellular S₀ globule production and degradation in *Chlorobaculum tepidum* via dynamic cell-globule interactions. *Microbiology (Reading)*, 162, 1125–1134.
- Mamocho, C.L., Sabanayagam, C.R., Modla, S., Powell, D.H., Henri, P.A., Steele, A.S. et al. (2019) Insights into the mineralogy and surface chemistry of extracellular biogenic S(0) globules produced by *Chlorobaculum tepidum*. *Frontiers in Microbiology*, 10, 271.
- Menin, L., Gaillard, J., Parot, P., Schoepp, B., Nitschke, W. & Verméglio, A. (1998) Role of HiPIP as electron donor to the RC-bound cytochrome in photosynthesis purple bacteria. *Photosynthesis Research*, 55, 6–348.
- Menin, L., Schoepp, B., Parot, P. & Verméglio, A. (1997) Photoinduced cyclic electron transfer in *Rhodocyclus tenuis* cells: participation of HiPIP or cyt c8 depending on the ambient redox potential. *Biochemistry*, 36, 12183–12188.
- Messner, C.B., Demichev, V., Wang, Z., Hartl, J., Kustatscher, G., Mulleder, M. et al. (2023) Mass spectrometry-based high-throughput proteomics and its role in biomedical studies and systems biology. *Proteomics*, 23, e2200013.
- Meyer, T.E. (1985) Isolation and characterization of soluble cytochromes, ferredoxins and other chromophoric proteins from the halophilic phototrophic bacterium *Ectothiorhodospira halophila*. *Biochimica et Biophysica Acta*, 806, 175–183.
- Murali, R., Gennis, R.B. & Hemp, J. (2021) Evolution of the cytochrome bd oxygen reductase superfamily and the function of CydAA' in archaea. *ISME Journal*, 15, 3534–3548.
- Ohmine, M., Matsuura, K., Shimada, K., Alric, J., Verméglio, A. & Nagashima, K.V. (2009) Cytochrome c4 can be involved in the photosynthetic electron transfer system in the purple bacterium *Rubrivivax gelatinosus*. *Biochemistry*, 48, 9132–9139.
- Oremland, R.S., Saltikov, C.W., Stolz, J.F. & Hollibaugh, J.T. (2017) Autotrophic microbial arsenotrophy in arsenic-rich soda lakes. *FEMS Microbiology Letters*, 364(15), fnx146.
- Pelosi, L., Vo, C.D., Abby, S.S., Loiseau, L., Rascalou, B., Hajj Chehade, M. et al. (2019) Ubiquinone biosynthesis over the entire O₂ range: characterization of a conserved O₂-independent pathway. *MBio*, 10(4), e01319–19.
- Planer-Friedrich, B., Hartig, C., Lohmayer, R., Suess, E., McCann, S.H. & Oremland, R. (2015) Anaerobic chemolithotrophic growth of the haloalkaliphilic bacterium strain MLMS-1 by disproportionation of monothioarsenate. *Environmental Science & Technology*, 49, 6554–6563.
- Planer-Friedrich, B., London, J., McCleskey, R.B., Nordstrom, D.K. & Wallschläger, D. (2007) Thioarsenates in geothermal waters of Yellowstone National Park: determination, preservation, and geochemical importance. *Environmental Science & Technology*, 41, 5245–5251.
- Porat, I., Waters, B.W., Teng, Q. & Whitman, W.B. (2004) Two biosynthetic pathways for aromatic amino acids in the archaeon *Methanococcus maripaludis*. *Journal of Bacteriology*, 186, 4940–4950.
- Pott, A.S. & Dahl, C. (1998) Sirohaem sulfite reductase and other proteins encoded by genes at the *dsr* locus of *Chromatium vinosum* are involved in the oxidation of intracellular sulfur. *Microbiology (Reading)*, 144(Pt 7), 1881–1894.
- Qing, C., Nicol, A., Li, P., Planer-Friedrich, B., Yuan, C. & Kou, Z. (2023) Different sulfide to arsenic ratios driving arsenic speciation and microbial community interactions in two alkaline hot springs. *Environmental Research*, 218, 115033.
- Raturi, G., Chaudhary, A., Rana, V., Mandlik, R., Sharma, Y., Barvkar, V. et al. (2023) Microbial remediation and plant-microbe interaction under arsenic pollution. *Science of the Total Environment*, 864, 160972.
- Raymond, J.C. & Sistrom, W.R. (1969) *Ectothiorhodospira halophila*: a new species of the genus *Ectothiorhodospira*. *Archives in Microbiology*, 69, 121–126.
- Richey, C., Chovanec, P., Hoefft, S.E., Oremland, R.S., Basu, P. & Stolz, J.F. (2009) Respiratory arsenate reductase as a bidirectional enzyme. *Biochemical and Biophysical Research Communications*, 382, 298–302.
- Ross, D.E., Ruebush, S.S., Brantley, S.L., Hartshorne, R.S., Clarke, T.A., Richardson, D.J. et al. (2007) Characterization of protein-protein interactions involved in iron reduction by *Shewanella oneidensis* MR-1. *Applied Environmental Microbiology*, 73, 5797–5808.
- Schoepp-Cothenet, B., Lieutaud, C., Baymann, F., Verméglio, A., Friedrich, T., Kramer, D.M. et al. (2009) Menaquinone as pool quinone in a purple bacterium. *Proceedings of National Academy of Sciences United States of America*, 106, 8549–8554.
- Schwanhauser, B., Busse, D., Li, N., Dittmar, G., Schuchhardt, J., Wolf, J. et al. (2011) Global quantification of mammalian gene expression control. *Nature*, 473, 337–342.



- Shi, K., Wang, Q. & Wang, G. (2020) Microbial oxidation of arsenite: regulation, chemotaxis, phosphate metabolism and energy generation. *Frontiers in Microbiology*, 11, 569282.
- Soufi, B. & Macek, B. (2015) Global analysis of bacterial membrane proteins and their modifications. *International Journal of Medical Microbiology*, 305, 203–208.
- Stoffels, L., Krehenbrink, M., Berks, B.C. & Uden, G. (2012) Thiosulfate reduction in *Salmonella enterica* is driven by the proton motive force. *Journal of Bacteriology*, 194, 475–485.
- Szyttenholm, J., Chaspoul, F., Bauzan, M., Ducluzeau, A.L., Chehade, M.H., Pierrel, F. et al. (2020) The controversy on the ancestral arsenite oxidizing enzyme; deducing evolutionary histories with phylogeny and thermodynamics. *Biochimica et Biophysica Acta*, 1861, 148252.
- Tedro, S.M., Meyer, T.E. & Kamen, M.D. (1985) Amino acid sequence of high-redox-potential ferredoxin (HiPIP) isozymes from the extremely halophilic purple phototrophic bacterium, *Ectothiorhodospira halophila*. *Archives of Biochemistry and Biophysics*, 241, 656–664.
- ten Brink, F., Schoep-Cothenet, B., van Lis, R., Nitschke, W. & Baymann, F. (2013) Multiple Rieske/cytb complexes in a single organism. *Biochimica et Biophysica Acta*, 1827, 1392–1406.
- Tikhonova, T.V., Liliina, A.V., Osipov, E.M., Shipkov, N.S., Dergousova, N.I., Kulikova, O.G. et al. (2021) Catalytic properties of flavocytochrome c sulfide dehydrogenase from haloalkaliphilic bacterium *Thioalkalivibrio paradoxus*. *Biochemistry (Mosc)*, 86, 361–369.
- Trueper, H.G. & Schlegel, H.G. (1964) Sulphur metabolism in *Thiorhodaceae*. I. Quantitative measurements on growing cells of *Chromatium Okenii*. *Antonie Van Leeuwenhoek*, 30, 225–238.
- Tyanova, S. & Cox, J. (2018) Perseus: a bioinformatics platform for integrative analysis of proteomics data in cancer research. *Methods in Molecular Biology*, 1711, 133–148.
- van Lis, R., Nitschke, W., Duval, S. & Schoep-Cothenet, B. (2013) Arsenics as bioenergetic substrates. *Biochimica et Biophysica Acta*, 1827, 176–188.
- Weissgerber, T., Sylvester, M., Kroninger, L. & Dahl, C. (2014) A comparative quantitative proteomic study identifies new proteins relevant for sulfur oxidation in the purple sulfur bacterium *Allochromatium vinosum*. *Applied Environmental Microbiology*, 80, 2279–2292.
- Wells, M., McGarry, J., Gaye, M.M., Basu, P., Oremland, R.S. & Stolz, J.F. (2019) Respiratory selenite reductase from *Bacillus selenitireducens* strain MLS10. *Journal of Bacteriology*, 201(7), e00614–e00618.
- White, G.F., Edwards, M.J., Gomez-Perez, L., Richardson, D.J., Butt, J.N. & Clarke, T.A. (2016) Mechanisms of bacterial extracellular electron exchange. *Advances in Microbial Physiology*, 68, 87–138.
- Yamagata, S. (1989) Roles of O-acetyl-L-homoserine sulfhydrylases in micro-organisms. *Biochimie*, 71, 1125–1143.
- Zargar, K., Conrad, A., Bernick, D.L., Lowe, T.M., Stolc, V., Hoefft, S. et al. (2012) ArxA, a new clade of arsenite oxidase within the DMSO reductase family of molybdenum oxidoreductases. *Environmental Microbiology*, 14, 1635–1645.
- Zu, Y., Couture, M.M., Kolling, D.R., Crofts, A.R., Eltis, L.D., Fee, J.A. et al. (2003) Reduction potentials of Rieske clusters: importance of the coupling between oxidation state and histidine protonation state. *Biochemistry*, 42, 12400–12408.

SUPPORTING INFORMATION

Additional supporting information can be found online in the Supporting Information section at the end of this article.

How to cite this article: D'Ermo, G., Audebert, S., Camoin, L., Planer-Friedrich, B., Casiot-Marouani, C., Delpoux, S. et al. (2024) Quantitative proteomics reveals the Sox system's role in sulphur and arsenic metabolism of phototroph *Halorhodospira halophila*. *Environmental Microbiology*, 26(6), e16655. Available from: <https://doi.org/10.1111/1462-2920.16655>